PART I
AN X-RAY CRYSTALLOGRAPHIC
STRUCTURE DETERMINATION
OF BROMOMALONAMIDE

PART II
AM ESR STUDY OF RADICALS IN
SINGLE CRYSTALS OF *- IRRADIATED
BROMOMALONAMIDE AND
IODOACETAMIDE

Dissertation for the Degree of Ph. D.
MICHIGAN STATE UNIVERSITY
ROBERT FRANCIS PICONE
1973



This is to certify that the

thesis entitled

Part I. An x-ray Crystallographic Structure Determination of Bromomalonamide. Part II. An ESR Study of Radicals in Single Crystals of $\gamma\text{-irradiated}$ Bromomalonamide and Iodoacetamide.

presented by

Robert Francis Picone

has been accepted towards fulfillment of the requirements for

PH.D. degree in Chemistry

Major professor

Date 12/12/73

O-7639



ABSTRACT

PART I

AN X-RAY CRYSTALLOGRAPHIC STRUCTURE DETERMINATION OF BROMOMALONAMIDE

PART II

AN ESR STUDY OF RADICALS IN SINGLE CRYSTALS OF γ -IRRADIATED BROMOMALONAMIDE AND IODOACETAMIDE

Ву

Robert Francis Picone

No carbon-centered radicals with bromine or iodine substituents had previously been studied by single-crystal ESR methods. The purpose of this work was to obtain examples of such radicals, carry out analyses of their ESR spectra and use the ESR parameters to deduce their structures. In order to interpret the ESR spectra of single crystals in the most thorough manner, crystallographic data are desirable for the host crystal. It proved necessary to obtain such information in this work since no previous crystallographic investigations of the materials used had been carried out. The principal results of this investigation are summarized below:

I. The crystal structure of bromomalonamide, $\mathrm{HBrC}(\mathrm{CONH_2})_2$, has been determined from MoK_α diffractometer data by use of Patterson and Fourier syntheses. The crystals are

6 87831

orthorhombic, Pnma, with cell constants at 22° : \underline{a} = $9.487(3)^{\circ}A$, \underline{b} = $11.294(4)^{\circ}A$, \underline{c} = $5.885(3)^{\circ}A$, ρ_{C} = 1.90 g cm⁻³, ρ_{m} = 1.85 g cm⁻³. The value of R_{1} for 270 observed reflections is 0.029. There are four molecules in the unit cell and one-half molecule in the asymmetric unit. The bond lengths are C-Br, $1.954(5)^{\circ}A$; C=0, $1.236(7)^{\circ}A$; C-N, $1.290(5)^{\circ}A$; C-C, $1.522(9)^{\circ}A$. The three-dimensional hydrogen bonding network contains eight- and twelve-membered rings with N....0 distances of 2.94(1) and $2.82(1)^{\circ}A$, and H....0 distances of 2.21(7) and $1.85(7)^{\circ}A$, respectively; the N-H...0 angles are $164(7)^{\circ}A$. A rigid body analysis of the thermal motions indicates that there is a librational motion, dominated by the hydrogen bonding scheme, of about $7^{\circ}A$ about a line joining the amide nitrogens of a molecule.

II. Both powder and single-crystal ESR spectra of paramagnetic species formed by γ-irradiation of bromomalonamide at 770K have been obtained. One radical shows a large bromine hyperfine interaction plus a small proton interaction and g, A(81Br) and e²qQ(81Br) tensors have been determined from an analysis of the spectra of the deuterated form. The data have been interpreted as favoring the structure ·CHBrCONH₂ for this species. The second fragment has been identified as ·CONH₂ but ESR parameters are not reported since it has been studied previously. Neither species is stable at room temperature in the host crystal.

III. Powder and single-crystal ESR spectra of iodoacetamide, γ -irradiated and observed at $77^0\mathrm{K}$, have been analyzed. Hyperfine interaction with one iodine and one hydrogen nucleus is observed and the $\mathrm{A}(^{127}\mathrm{I})$, $\mathrm{A}(\mathrm{H})$, g and $\mathrm{e}^2\mathrm{qQ}(^{127}\mathrm{I})$ tensors have been found. These data indicate that the radical species is the π -electron radical, 'CHICONH₂, and are consistent with a planar or nearly planar structure. The g and $\mathrm{A}(^{127}\mathrm{I})$ tensors are axial, or nearly so. The odd-electron spin densities in the iodine 5s and $\mathrm{5p}_{\pi}$ orbitals are larger than found for the halogens in the analogous fluoro-and chloro-radicals, but are comparable with the values found for bromine in 'CHBrCONH₂.

PART I

AN X-RAY CRYSTALLOGRAPHIC STRUCTURE DETERMINATION OF BROMOMALONAMIDE

PART II

AN ESR STUDY OF RADICALS IN SINGLE CRYSTALS OF γ -IRRADIATED BROMOMALONAMIDE AND IODOACETAMIDE

Ву

Robert Francis Picone

A DISSERTATION

Submitted to
Michigan State University
in partial fulfillment of the requirements
for the degree of

DOCTOR OF PHILOSOPHY

Department of Chemistry

1973

то

My Parents

ACKNOWLEDGMENTS

The author wishes to express his appreciation to Professor M. T. Rogers for his encouragement and numerous helpful discussions during the course of this project. The author is also grateful to Dr. Mel Neuman for his patience and guidance during the X-ray crystallographic work. Thanks is also due to Dr. William Waller for assistance with computer programs used for this study and to Dr. S. Subramonian for discussions and assistance.

TABLE OF CONTENTS

						Page
PART	I.	AN X-RAY CRYSTALLOGRAPHIC STRUCTURE DETERMINATION OF BROMOMALONAMIDE .		•	•	1
I.	INI	TRODUCTION	o •	•	•	1
II.	CRY	STALLOGRAPHY		•	•	3
III.	THE	E X-RAY EXPERIMENT		•	•	5
	Α.	Bragg's Law		•	•	5
	В.	Data Collection		•		7
	c.	Data Correction		•	•	9
IV.	THE	CORETICAL		•	•	11
	Α.	Phase Problem		•	•	11
	В.	Structure Factor		•	•	13
		1. Scattering Factor		•	•	16
		2. The Temperature Factor		•		16
		3. Anomalous Dispersion			•	18
	C.	Patterson or Heavy Atom Methods			•	19
	D.	Least—Squares Methods		•	•	27
V.	EXE	PERIMENTAL PROCEDURES	, •	•	•	31
	Α.	Preparation of Bromomalonamide		•	•	31
	В.	Selection and Alignment of Crystals	•	•	•	32
	c.	Precession Techniques			•	34
	D.	Diffractometer		•	•	37
	E •	Data Processing		•	•	3 9
	F.	Patterson and Fourier Maps			•	41

TABLE OF CONTENTS (Cont.)

	·																		Page
VI.	RES	SULTS	AND	DIS	cuss	ION	I	•	•	•	•	•	•	•	•	•	•	•	45
	Α.	Mole	culai	: Ge	omet	ry	•	•	•	•	•	•		•	•	•	•		45
	В.	Ther	mal N	1oti	ons	•	•	•	•	•	•		•	•	•	•	•	•	52
PART	II.		ESR S													RY	'SI	'AL	S
			γ-IRF OACEI			• BF	·	·	·	·	·	•)E	•	•	•	•	•	57
I.	INI	RODU	CTION	ı .		•	•	•	•	•		•	•	•	•	•	•	•	57
II.	ד.דיז	ERATI	IRE S	SURV	EY -		_		_	_		_	_		_	_	_	_	63
						•	•	•	•	•	•	•	•	•	•	•	•	•	
III.	THE	E ESR	EXPE	ERIM	ENT	•	•	•	•	•	•	•	•	•	•	•	•	•	65
IV.	THE	EORY	• •		• •	•	•	•	•	•	•	•	•	•	•	•	•	•	68
	Α.	Spin	Hami	lto	nian	. •	•		•	•	•	•	•	•	•	•	•	•	68
	В.	Appro	oxima	ate	Solu	tic	ns	3	•	•	•	•	•	•	•	•	•	•	73
V.	TEC	CHNIQ	UES			•	•	•	•	•	•	•	•		•	•	•	•	81
	Α.	Sing	le-Cr	yst	al S	pec	tr	a				•			•	•	•	•	81
	в.	Powde	er Sp	ect	ra .	•	•	•			•	•	•		•	•	•	•	82
	C.	Solu	tion	Spe	ctra	•	•	•	•	•	•	•	•	•	•	•	•	•	83
VI.	НУЕ	PERFI	NE IN	TER	ACTI	ONS	,	•	•	•	•	•	•		•	•	•	•	85
	Α.	α-Pro	oton	Cou	plin	g				•	•			•	•			•	85
	В.	β-Pro		•		-		•			•	•	•	•	•	•	•	•	87
	C.	Nitro	ogen-	-and	Ami	de-	-Pr	ot	on	C	ou	ıpl	in	g	•	•	•	•	91
	D.	α-Flu	uorir	ne C	oupl	ing	ſ	•	•		•	•	•	•	•	•	•	•	91
	E •	α -Ch	lorir	ne C	oupl	ing	ſ	•	•	•	•	•	•	•	•	•	•	•	9 3
VII.	EXI	PERIM	ENTAI	٠ .		•	•	•	•	•	•	•	•	•	•	•	•	•	96
	Α.	Prepa	arati	lon,	Cry	sta	1	Gr	OW	/th	n a	and	lc	ry	st	:a1	. –		
		logra		• •	• •	•	•	•	•	•	•	•	•	•	•	•	•	•	96
	В.	Samp	_					ic	n	Pr						•	•	•	99
	c.	Spec			_			•	•	-		•					•	•	102
	D.	Conve	ersid	on F	acto	rs											•	•	104

TABLE OF CONTENTS (Cont.)

													Page
VIII. R	ESULT	S AND DIS	CUSSION		•		•	•	•	•	•	•	105
Α.	Brom	omalonami	de		•		•	•	•	•	•	•	105
	1.	Powder S	pectra		•		•	•	•	•	•	•	105
	2.	Single-C	rystal	Spec	tra	•	•		•	•	•	•	108
	3.	Structur	e of th	e Ra	dic	al	•	•	•	•	•	•	117
	4.	Other Co	nsidera	tion	ıs		•	•	•	•	•	•	121
В.	Iodo	acetamide			•		•	•		•	•	•	123
	1.	Powder S	pectra				•	•	•	•	•	•	123
	2.	Single-C	rystal	Spec	tra	•	•	•		•		•	125
	3.	g and	A(1271)	Ten	sor	s.	•	•	•	•			127
	4.	A(H) Ten	sor		•		•	•	•	•		•	132
	5.	Quadrupo										•	132
	6.	Structur	e of th	e Ra	dic	al	•	•		•	•		132
T35 C													135
IX. S	UMMAR	Y • • •	• • • •	• •	•	• •	•	•	•	•	•	•	133
REFERENC	ES												
PAR	TI.				•		۰	•		•	•	•	136
מגם	m TT												127

LIST OF TABLES

PART I

TABLE		Page
ı.	Symmetry relationships of space group Pnma .	24
II.	Patterson vectors for bromine in space group Pnma	25
III.	Experimental sequence for bromomalonamide structure determination	30
IV.	Observed and calculated structure factors for bromomalonamide (all values x 10)	44
V.	Interatomic distances and angles	47
VI.	Structural parameters for diamides	48
VII.	Atomic coordinates and thermal parameters for bromomalonamide. The anisotropic thermal parameters are defined as $[-(\beta_{11}h^2 + \beta_{22}k^2 + \beta_{33}\ell^2 + 2\beta_{12}hk + 2\beta_{13}h\ell + 2\beta_{23}k\ell)]$	53
VIII.	Translational and librational matrices for thermal motions in bromomalonamide	54
	PART II	
ı.	Representative α -proton hyperfine interactions	89
II.	Representative β -proton hyperfine interactions	89
III.	Representative α -fluorine hyperfine interactions	94
IV.	Representative α -chlorine hyperfine interactions	94

LIST OF TABLES (Cont.)

TABLE		Page
٧.	ESR parameters for the 'CHBr(CONH ₂) and CDBr(CONH ₂) radicals	107
VI.	Components of the halogen hyperfine splitting tensors and spin densities in haloacetamide radicals	118
VII.	ESR parameters for the radical ${}^{\bullet}\mathrm{CHICONH_2}$.	131
VIII.	Components of the iodine hyperfine splitting tensor and spin densities in the iodine valence orbitals	ce 133

LIST OF FIGURES

PART I

Figure		Page
1.	Scattering factor curve for carbon	17
2.	Crystal axes of bromomalonamide	33
3.	Stereographic view of bromomalonamide	46
4.	Stereographic view of the hydrogen bonding of bromomalonamide	50
	PART II	
1.	 a) First-order energy levels and allowed transitions; b) Second-order energy levels and allowed transitions	78
2.	Spin polarization of a C-H bond in a π -electron radical	88
3.	Axis system of iodoacetamide crystal	97
4.	First derivative X-band ESR spectra of bromomalonamide powder γ-irradiated and observed at 77°K: a) irradiated CHBr(CONH ₂) ₂ , b) irradiated CDBr(CONH ₂) ₂ . The upper set of arrows indicates the parallel, and the lower the perpendicular, line positions	f set 106
5.	Second-derivative single-crystal ESR spectrum of CDBrCOND ₂ with the magnetic field along the a crystallographic axis. Arrow indicate the •COND ₂ radical	es 109
6.	Second-derivative single-crystal ESR spectrum of CDBrCOND ₂ with the magnetic field along the b crystallographic axis	110

LIST OF FIGURES (Cont.)

Figure		Page
7.	Second-derivative ESR single-crystal spectrum of CDBrCOND ₂ . The stick diagrams show the line positions and intensities calculated with the complete Hamiltonian for: a) $q_{zz} _{A (Br)}$	i :), 111
8.	Isofrequency plot of line positions of $^{81}\mathrm{Br}$ in the bc plane of bromomalonamide	112
9.	Isofrequency plot of line positions of $^{81}\mathrm{Br}$ in the ac plane of bromomalonamide	113
10.	Isofrequency plot of line positions of $^{81}\mathrm{Br}$ in the ab plane of bromomalonamide	114
11.	X-band powder spectrum of irradiated iodo- acetamide. The arrows indicate the ¹²⁷ I parallel hyperfine line position	124
12.	X-band second-derivative ESR spectrum of a single crystal of irradiated iodoacetamide. The magnetic field is along the b axis	126
13.	Isofrequency plot of line positions of ¹²⁷ I in the bc plane of iodoacetamide	128
14.	Isofrequency plot of line positions of ¹²⁷ I in the a*c plane of iodoacetamide	129
15.	Isofrequency plot of line positions of 127 I in the a*b plane of iodoacetamide	130

PART I

AN X-RAY CRYSTALLOGRAPHIC STRUCTURE DETERMINATION OF BROMOMALONAMIDE

I. INTRODUCTION

Crystallography, as a science, dates back several centuries. The investigations at that time were necessarily limited to the observations concerning the external features of crystals. From these early enquiries, it was soon postulated that the regular and symmetrical arrangment of crystal faces was due to some sort of internal pattern. Following the discovery of X-rays in 1895 by Roentgen, experimentalists were given the means to explore these ideas and examine the internal structure of crystals. It was not until 1912 that the utility of X-rays was perceived. von Laue postulated that X-rays are of the same order of magnitude as the interatomic spacings in a crystal. Hence, the crystal could act as a three-dimensional diffraction grating and diffract a beam of X-rays. In that same year Friedrich and van Knippering confirmed this idea experimentally. Shortly thereafter in 1913, W. L. Bragg worked out the first crystal structure. In recent years the development of the computer and the automated diffractometer

have brought the science of crystallography within the reach of any scientist who avails himself of these instruments.

Determination of the crystal structure of bromomalonamide was undertaken to aid in the interpretation of the ESR
data for the radical which is obtained on irradiating the
amide. In a similar type of investigation the crystal
structure of malonamide has been obtained and used in discussing the ESR spectra of radicals trapped in irradiated
single crystals of this substance. 1-3

X-ray crystal analyses have been reported for three additional diamides, oxamide, succinamide and dichloromalonamide. The structures in all cases involve important intermolecular hydrogen bonding but the conformations of the molecules, and the arrangements in the three-dimensional networks, differ. An analysis of the thermal motions in bromomalonamide has also been made in this work.

II. CRYSTALLOGRAPHY

A crystal may be defined as a solid composed of some basic internal pattern which repeats itself at periodic intervals. The fundamental building block is referred to as the unit cell. The unit cell is a parallelopiped which consists of an atom, ion, molecule or some combination thereof. Under a set of translation operations, the unit cell will fill the entire crystal volume. The contents of the unit cell may, in turn, be generated from appropriate symmetry operations on the asymmetric unit, the unique portion of the unit cell. In crystallography it is usual to solve for the crystal structure in terms of the asymmetric unit rather than the entire unit cell. This considerably simplifies the task of the crystallographer.

The symmetry relationships consist of the familiar molecular symmetry elements: mirror planes, rotation axes, centers of inversion, and rotation-reflection axes. In addition, two new elements, screw axes and glide planes, result from the translational operations of crystal symmetry. A screw axis is a rotation about an axis followed by a translation parallel to the axis. A glide plane is a mirror in the plane followed by a translation parallel to the plane.

There are several types of unit cells commonly encountered in crystallographic work. The primitive (P) cell is a minimum volume cell with lattice points at each corner. The body centered (I) and face centered (F) cells are self-explanatory.

If each unit cell were to be replaced by a representative point and the points were to be connected, a crystal lattice would be formed. The direct lattice would be quite useful if a real image, such as the image provided by a microscope, were obtained, since the direct lattice is associated with real space and a relatively simple relationship between the crystal structure and the lattice would result. However, in X-ray crystallography, it is the diffracted image which is produced. This is a map of the reciprocal lattice rather than the direct lattice. The reciprocal lattice is associated with Fourier space. 9 The reciprocal and direct lattice have the same symmetry and are simply related to each other. For a lattice with axes a, b, c there is a related second lattice such that a*, is to a and c, b* is | to a and c, and c* is to a and b.

III. THE X-RAY EXPERIMENT

A. Bragg's Law

When a beam of X-rays strikes a crystal most of the beam passes through the crystal unaffected. A small amount of the beam, though, is scattered by the atoms which constitute the crystal, creating a diffraction pattern. Scattering occurs when the electrons act as secondary sources of radiation (the incident beam is the primary source) and emit X-rays in all directions. The frequency and wavelength of the emitted X-rays are the same as those of the incident beam. An analogy is sometimes drawn between diffraction and ordinary optical reflection. Since the diffracted beam appears to be a reflection from a lattice plane, it is often referred to as a reflection. W. L. Bragg first noticed the similarity between the two processes and developed a particularly simple equation to describe the diffraction phenomenon subject to the following considerations:

- The angle of the diffracted beam equals the angle of the incident beam.
- 2) Waves from successive parallel planes must arrive at a detector in phase in order to produce an intensity maximum.
- 3) The distance traveled by the waves must equal some integral number of wavelengths in order for the waves to be in phase.

The Bragg equation is

$$\sin \theta = \frac{n\lambda}{2d} , \qquad (1)$$

where θ is the angle of "reflection", λ is the wavelength of the incident radiation in \hat{A} , n is an integer which gives the order of the reflection, d is the interplanar spacing in the crystal lattice in \hat{A} .

Bragg's law leads to several conclusions:

- 1) θ and λ must be matched before a reflection can be observed. An X-ray beam at an arbitrary angle with respect to the crystal will not necessarily give a diffraction pattern. In practice, the diffraction angle is varied until the crystal is properly aligned in the X-ray beam to satisfy Bragg's law.
- 2) The wavelength needed to produce a diffraction pattern must be approximately the same dimension as the interplanar spacing. This corresponds to the X-ray region of the electromagnetic spectrum,

- 0.1 to 100 Å and the region of most concern is about 1 Å. Radiation of longer wavelength will result in poor resolution while radiation of shorter wavelength will result in a scattering angle too small to be conveniently measured.
- 3) Since there is an inverse proportionality between d and $\sin \theta$ it is more convenient to use the reciprocal lattice. There is then a direct relationship between $\sin \theta$ and d^* .

B. Data Collection

A precession or an oscillation camera is used for the alignment, unit cell measurements and space group determination. Although the two methods are complementary, usually one or the other is used exclusively in the initial datacollecting stages. The Polaroid precession camera has the advantage in the speed with which the crystal may be aligned. The precession camera makes a complicated series of motions involving the camera and film to give a photographic image of the reciprocal lattice. Since the wavelength of radiation is selected beforehand, and the diffracted angle is an easily determined experimental parameter, the reciprocal lattice spacings may be obtained by applying the Bragg equation. The reciprocal lattice spacings are readily converted to the direct lattice spacings, which, in turn, will yield the dimensions of the unit cell axes.

The space group is determined from the systematic absences among the reflections on the photographs. The choices of space groups for combinations of h k l extinctions are listed in the International Tables for X-ray Crystallography, Volume I.¹⁰

The X-ray experiment is capable of detecting only translational symmetry elements¹¹ and in addition adds a center of symmetry to a crystal whether it is present or not. Therefore a unique selection of the space group is not always possible from photographs.

Although a centric crystal can be distinguished from an acentric one by the piezoelectric effect, it is not a very reliable indicator. However, from the complete crystal structure analysis, the correct space group assignment can be conclusively made.

Film methods may be used to record all of the X-ray intensity data. The process is tedious and subject to human error when the intensities are judged. In recent years, therefore, data collection has become almost completely automated. A computer-controlled diffractometer is used to measure the intensities by moving the scintillation counter and crystal to the appropriate location in space. The reflection is then measured as a function of time. With a diffractometer the data is collected with more speed and accuracy than is possible with film techniques. The entire procedure ranges from several days for a simple crystal system to a few weeks for a more complicated system.

C. Data Correction

The raw intensities obtained from the scintillation counter have to be adjusted before the data can be used in structure calculations.

If the crystal absorbs radiation of the wavelengths selected, then an absorption correction, <u>abs</u>, has to be performed. Since this process is time consuming and expensive, it is usually omitted for those compounds with a small mass absorption coefficient.

The correction is accomplished <u>via</u> a computer program based on some variation of Beer's law,

$$I = I_0 \exp(-\rho \left(\frac{\mu}{\rho}\right)_{\lambda} \tau), \qquad (2)$$

where I is the intensity of the X-ray beam passing through a crystal of thickness τ , I₀ is the intensity of the incident beam, ρ is the density of the compound, and $(\frac{\mu}{\rho})_{\lambda}$ is the mass absorption coefficient, which is dependent on the wavelength of the X-rays. Values of $(\frac{\mu}{\rho})_{\lambda}$ are tabulated in the International Tables for X-ray Crystallography, Volume III.¹²

Another effect which must be taken into account is the Lorentz factor. This correction is a consequence of the diffraction geometry, and the form applicable to the intensity measurements made from a diffractomer is:

$$L = \frac{1}{\sin 2\theta} . \tag{3}$$

The final correction term is the polarization factor.

It is not dependent on the manner in which the data are collected. The incident beam is unpolarized but the reflected beam from the crystal is partially polarized. This is taken into account by the polarization factor p, which is

$$P = \frac{1 + \cos^2 \theta}{2} \quad . \tag{4}$$

Often these latter two equations are combined, since they are a function of 2θ , into a single Lorentz-polarization factor

$$LP = \frac{1 + \cos^2 2\theta}{2\sin 2\theta} . \tag{5}$$

The computation of the absorption and Lorentz-polarization factors involves no knowledge of the structure and is carried out before the data are refined. Collectively these corrections are referred to as geometric factors.

In a typical crystal structure, several hundred reflections are collected. The corrections, with their dependence on θ , have to be calculated for each θ value. This rather tedious process is readily adaptable to computer techniques. Prior to the development of rapid computers with large memories, crystallographers were reluctant to undertake absorption corrections. Computers, therefore, have not only contributed to more crystal structures being solved but also to more accurate crystal structures.

IV. THEORETICAL

A. Phase Problem

The main objective of crystallography is to take the diffracted image produced by the X-ray beam and attempt to reconstruct the arrangement of atoms in the unit cell which led to that particular diffraction pattern. The quantity which is measured in a crystallographic experiment and which contains part of this information is the intensity of the reflections. The intensity is simply related to the square of the amplitude of the diffracted waves. In order to piece together the unit cell contents from the diffraction data, however, it is necessary to know both the amplitude and the phase. The phase information is lost in the process of data collection. Therefore, a major concern of crystallographers, at present, is the regeneration of this lost phase information.

For a crystal whose unit cell lacks a center of symmetry (acentric), the diffracted waves may be anywhere from 0° to 180° out of phase. For a crystal whose unit cell contains a center of symmetry (centric or centrosymmetric), there are only two possibilities for the phase angle. Either the wave is in phase (+) or it is 180° out of phase (-).¹³ The phase problem is immensely simplified, therefore, if a crystal has a center of symmetry. Nonetheless, the sheer number of reflections obtained from even a small crystal system (less than 50 atoms) makes calculations prohibitive without

the use of high-speed computer. For instance, a molecule with 300 observed reflections will have $(2)^{300}$ possible combinations of phase angles. With the aid of computers, though, problems of many times this magnitude can be solved routinely.

Much theoretical effort has been directed toward solving the phase problem since, in principle, all the structural information is present in the collected data, but the phase information cannot be extracted. This makes for an interesting theoretical problem. At present, though, there are only two practical ways, plus innumerable variations of each, of solving the crystal structure.

The Patterson method is applicable if the structure has a heavy atom from which the phases can be determined. If a heavy atom is not present, then isomorphous replacement, in which a heavy atom derivative is prepared, is a possibility. The unit cell must not be altered by the substitution. The structure of the heavy-atom derivative can then be solved and from it that of the original compound.

The direct-method attack is used if no heavy atom is present in the molecule. Such is the case with many organic crystals. Direct methods depend on the fact that the electron density is positive throughout the unit cell and are based on probable phase relationships for each reflection.

Much of this work has been pioneered by Harker and Kasper 14 and also by Sayres. This approach is most applicable to centrosymmetric structures.

B. Structure Factor

A function which relates the experimental data to the electron density is required in order to obtain a solution to the crystal structure. Such a function would have to be represented by a three-dimensional Fourier series, since the arrangement of atoms within the crystal is periodic. These requirements are fulfilled by the structure factor, a periodic function which is a mathematical description of the scattering of the waves by the atoms in the unit cell. The structure factor, $\mathbf{F}_{hk\ell}$, is composed of an amplitude and a phase. As was previously mentioned, the intensity is proportional to the square of the amplitude of the diffracted waves. The exact relationship between the amplitude of the reflection $|\mathbf{F}_{hk\ell}|$ and the intensity is:

$$I = |F_{hk}|^2 LP(abs)k , \qquad (6)$$

where the absorption (abs) and Lorentz-polarization (LP) factors are familiar from the section on data correction, and k is a proportionality or scaling constant. Its exact value is determined in the final stages of the structure determination.

There are numerous ways of representing the structure factor. In exponential form, it is written:

$$F_{hk\ell} = \sum_{j} |F_{hk\ell}| \exp(2\pi i (hx_{j} + ky_{j} + \ell z_{j}))$$

$$= \sum_{j} |F_{hk\ell}| \exp(i\alpha_{j})$$
(7)

 $|\mathbf{F}_{hk}|$ is the magnitude of the structure factor and α_j is the corresponding phase angle. The summation index, j, is equal to the number of atoms in the unit cell. The Miller indices, hk ℓ , serve the same purpose as the order of reflection, n, in the Bragg equation.

The structure factor may, alternatively, be presented in complex number form:

$$F_{hk\ell} = A_{hk\ell} + B_{hk\ell}$$

$$A_{hk\ell} = \sum_{j} f_{oj} \cos 2\pi (hx_j + ky_j + \ell z_j) = \sum_{j} f_{oj} \cos 2\alpha_j (9)$$

$$B_{hk\ell} = \sum_{j} f_{oj} \sin 2\pi (hx_j + ky_j + \ell z_j) = \sum_{j} f_{oj} \sin \alpha_j (10)$$

The magnitude, as expressed here, is:

$$|\mathbf{F}_{hk\ell}| = |\mathbf{A}_{hk\ell}^2 + \mathbf{B}_{hk\ell}^2|^{1/2}$$

$$= [\left(\sum_{j} \mathbf{f}_{oj} \cos \alpha_{j}\right)^2 + \left(\sum_{j} \mathbf{f}_{oj} \sin \alpha_{j}\right)^2]. (11)$$

The phase is:

$$\alpha_{j} = \tan^{-1}(\frac{B_{hk\ell}}{A_{hk\ell}}) = \tan^{-1}(\frac{\sum f_{oj} \sin \alpha_{j}}{\sum f_{oj} \cos \alpha_{j}}).$$
 (12)

For a centrosymmetric unit cell, the form of the structure factor can be represented by an even function, f(x) = f(-x). Hence, the sine terms will drop out and the equation reduces to:

$$\mathbf{F}_{hk\ell} = \sum_{j}^{\Sigma} \mathbf{f}_{oj} \cos \alpha_{j}.$$
 (13)

Since $f_{oj} \sin \alpha_j = 0$, then $\alpha_j = 0^0$ or 180° . No such simplification is possible for an acentric crystal.

The electron density can now be written as:

$$\rho(x,y,z) = V^{-1} \sum_{hk \ell} |F_{hk \ell}| \exp(-2\pi i (hx + ky + \ell z)).(14)$$

Defining a term, $\alpha'_{hk\ell} = \frac{\alpha_{hk\ell}}{2\pi}$, the density equation (14) may be rewritten:

$$\rho(\mathbf{x},\mathbf{y},\mathbf{z}) = \mathbf{v}^{-1} \sum_{\mathbf{h} \mathbf{k} \ell} |\mathbf{F}_{\mathbf{h} \mathbf{k} \ell}| \exp(-2\pi \mathbf{i}(\mathbf{h} \mathbf{x} + \mathbf{k} \mathbf{y} + \ell \mathbf{z} - \alpha'_{\mathbf{h} \mathbf{k} \ell})),$$

where V is the volume of the unit cell calculated from Bragg's law.

A closer examination of Equation 15 for the electron density which is in real space will reveal that it is merely the Fourier transform of the structure factor (Equation 7), which is in reciprocal space.

A trial crystal structure can now be assumed and the structure factors calculated on that basis. The agreement between the observed and the calculated structure factors will serve as a criterion for the correctness of the assumed structure. A quantity, R, the residual, is used for this purpose.

$$R = \frac{\sum ||F_{obs}| - |F_{calc}||}{\sum |F_{obs}|}$$
 (16)

1) The Scattering Factor

The f_O term encountered in the complex number form of the structure factor equation is known variously as the atomic scattering factor or the atomic form factor. The scattering power of an atom is a function of its electronic structure, the wavelength of X-radiation, and the angle of scatter. The scattering power reaches a maximum at $\theta = 0^{\circ}$ when the value of the form factor is equal to the atomic number of the scattering atom. Because at increasing values of θ , the scattered waves become increasingly out of phase with each other, the form factor will decrease with increasing $\theta = 0^{\circ}$ in $\theta = 0^{\circ}$. Figure 1 is a graphical representation of $\theta = 0^{\circ}$ versus $\theta = 0^{\circ}$ for a carbon atom, illustrating these features of the form factor. Values for the atomic form factors are listed in the International Table of X-Ray Crystallography, Volume III.12

2) The Temperature Factor

As presented in the above discussion, the scattering factor is independent of temperature. In the preliminary stages of the structure determination, this assumption is adequate. However, the atoms are not stationary but are vibrating about their equilibrium positions. This is a temperature dependent—phenomenon which has the net effect of decreasing the scattering factor. The modified form factor is

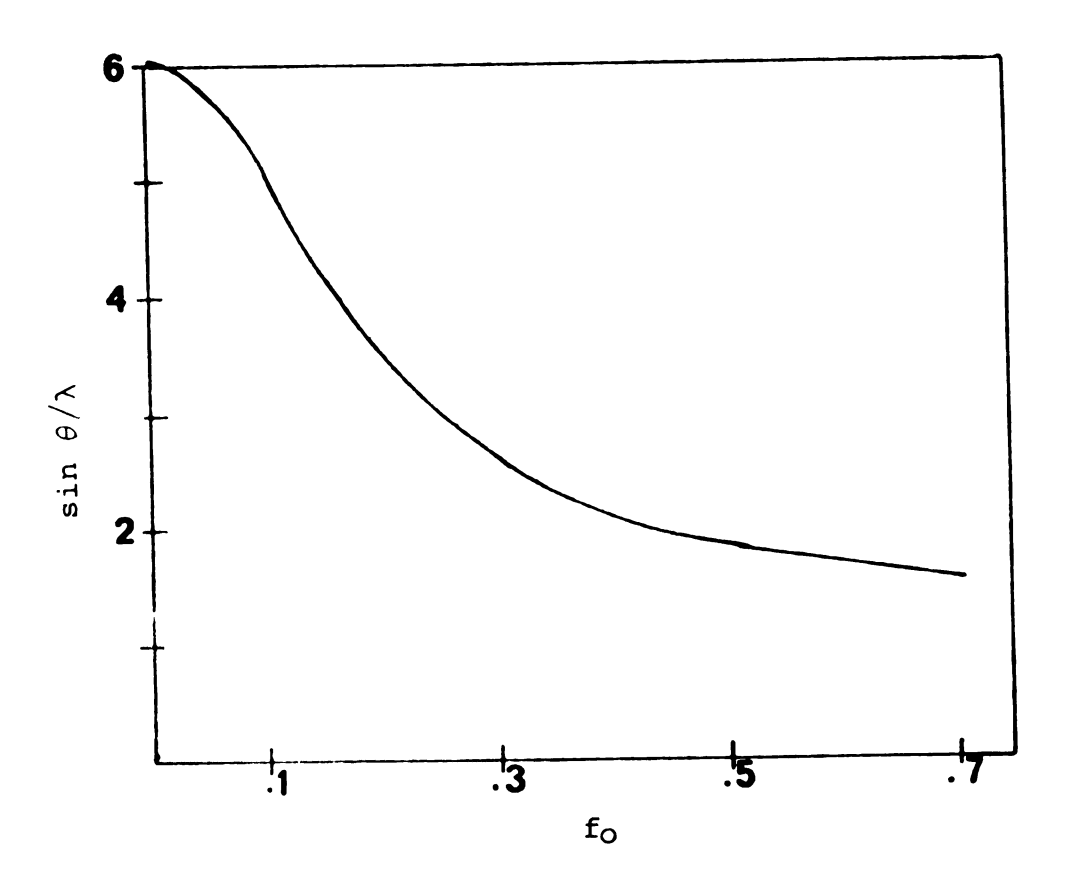


Figure 1. Scattering factor curve for carbon.

$$f = f_0 \exp(-\frac{B \sin^2 \theta}{\lambda^2})$$
, (17)

where B is known as the thermal or temperature factor. This factor is given by

$$B = 8\pi^2 \langle u_j^2 \rangle , \qquad (18)$$

where $\langle u_j^2 \rangle$ is the mean square vibration of the jth atom. Values of B for organic molecules typically range from 1 to 5.

The thermal motions can, in the simplest approximation, be treated isotropically. Usually the motions are considered as such until the refinement of the atomic coordinates stops at a given R value. Then the thermal motions are described anisotropically as a thermal ellipsoid. The R value will then reach a new minimum.

3) Anomalous Dispersion

In the event that the wavelength of the primary radiation is near an absorption edge of a scattering atom the phase of the scattered radiation will differ from that of the other atoms in the unit cell. This is referred to as anomalous scattering or anomalous dispersion. The effects are small and can be safely ignored if the structure consists only of light atoms such as carbon, oxygen, nitrogen, etc. However, if the structure contains a heavy atom such as bromine, the effects of anomalous dispersion cannot be disregarded.

The anomalous dispersion phenomenon can often be used to the advantage of the crystallographer. For instance, in the section on space group determination, it was mentioned that the X-ray experiment introduced a center of symmetry in the unit cell and, as a consequence, the hk ℓ reflections are equal to the $\bar{h}\bar{k}\bar{\ell}$ reflections (-h, -k, - ℓ). If anomalous dispersion effects occur then, for an acentric unit cell, the hk ℓ reflections are no longer equal to $\bar{h}\bar{k}\bar{\ell}$ reflections; however, for a centric structure the relation still holds.

With the inclusion of anomalous dispersion, the form factors are

$$f_{anom} = f_{o} + \Delta f' + i\Delta f'', \qquad (19)$$

where $\Delta f'$ is a real correction term and $\Delta f''$ is an imaginary quantity. Again values for f' and f'' may be obtained from the International Tables.¹²

C. Patterson or Heavy Atom Methods

An inherent difficulty in the electron density equation is the dependence on phase information which is unavailable. This obstacle is not insurmountable especially if the structure contains a heavy atom. The Fourier series is a weighted sum with the heavy atoms contributing the most to the structure factor. A truncated form of the Fourier series, involving only the heavy atoms could be written

$$F_{hk\ell} = \sum f_j^{heavy atoms} e^{-i\alpha} .16$$
 (20)

Naturally, this equation would not be correct. However, it would serve as a trial structure from which the positions of the other atoms could be obtained by an iterative procedure. This leads, though, to the initial problem of locating the heavy atom. Fortunately, there exists a powerful means of positioning the heavy atom without prior knowledge of the phase. A. L. Patterson in 1935 attempted to obviate the dependence on the phase relationship by using the squares of the magnitudes of the structure factors as Fourier coefficients. The Patterson function, P(u,v,w), is related only to the intensities of the diffracted waves and has a form quite similar to the electron density equation:

$$P(u,v,w) = V^{-1} \sum_{hk\ell} |F_{hk\ell}|^2 \exp[2\pi i (hu + kv + \ell w)], (21)$$

where u is the vector distance between atoms at x_1 , y_1 , z_1 , and x_2 , y_2 , z_2 , and w and v are defined analogously. The Patterson function produces a vector map of the interatomic distances for all of the atoms contained in the unit cell. In principle, the relative positions of the atoms can be derived from a Patterson map. Since a vector from A to B is equal in magnitude but opposite in direction to the vector from B to A, all Patterson maps are centrosymmetric. It was shown earlier that, for a centrosymmetric function, the Fourier series can be reduced to a sum of

cosine terms:

$$P(u,v,w) = V^{-1} \sum_{hk\ell} |F_{hk\ell}|^2 \cos 2\pi (hu + kv + \ell w). (22)$$

Another feature of the Patterson map is that all of the interatomic vectors of zero length, i.e. vectors from atoms to themselves, will lie at the origin resulting in a large peak. This can be used as a scaling factor to determine the relative heights of the peaks of the remaining vectors.

For a unit cell of N atoms, there are N^2 vectors in the Patterson; N of these are at the origin and $\frac{N(N-1)}{2}$ will be related to the remaining $\frac{N(N-1)}{2}$ by a center of inversion. Consequently a Patterson map will have $\frac{N(N-1)}{2}$ independent peaks. For a unit cell with even a moderate number of atoms, the peaks will overlap and result in an indistinguishable array of interatomic vectors. The magnitudes of the peaks, though, are proportional to the products of the atomic numbers of the two atoms forming the ends of the vector. A heavy atom among many light atoms is readily located. This is especially true if the symmetry requirements of the space group to which the crystal belongs are such that the heavy atom must be in a special position. Only those symmetry elements which involve no translational operations can lead to an atom being in a particular location. When an atom lies on a closed symmetry element such as a mirror plane, center of inversion, or rotation axis, then it is said to be in a special position of a space group. 17 These are fewer in number than the general positions but obey the same group symmetry.

As a specific example of the Patterson synthesis, consider the molecule bromomalonamide, HBrC(CONH₂)₂. space group is Pnma and there are four molecules (52 atoms) in the unit cell. According to the formulas given, the 52 atoms in the unit cell will result in 52 x 51 vector peaks. This is a large but not hopeless number of vectors to sort out. If the Patterson map were to be solved in its entirety, leading to the complete crystal structure of bromomalonamide, only $(52 \times 51)/2$ vectors would need to be found because of the centrosymmetric nature of the map. However, the usual situation is that one can locate only a few of the vectors, including those of the bromine. From the interatomic vectors which can be located the positions of the corresponding atoms can be determined. This information may then be used with the electron density function to phase the reflections. Since bromomalonamide is centrosymmetric, the phases will affect only the signs of the scattering factors.

The first vector to locate is the origin. This will have a height, ignoring the hydrogens, of:

 \times 6 \times 6 \times 6 \times 6 \times 6 \times 6).

A peak of this magnitude could perhaps obscure other nearby vectors. Some crystallographers, for this reason, consider

the origin to be of nuisance value and eliminate it from the map entirely. However, it can serve as a scale by which the peak heights of other vectors are judged. This is a definite advantage when trying to decide whether or not a peak is a composite of several overlapping vectors.

The largest vector peak, other than the origin, is the bromine-bromine vector. The relative height of this peak as compared to, say, the oxygen-oxygen vector is $\frac{35 \times 35}{8 \times 8}$, or it is about 20 times as intense. This indicates that the bromine-bromine vector will be easily discernible. examination of the symmetry table for the Pnma reveals that there are eight general equivalent positions. Since there are only four bromine atoms in the unit cell, these will occupy the special positions listed beneath the general positions in Table I. The possibilities for the special position include a mirror plane and one of two centers of inversion. The latter choices are clearly impossible so the bromine is located on the mirror plane. These four positions are:

1.
$$x, 1/4, z$$

1.
$$x$$
, $1/4$, z 3. $1/2 - x$, $3/4$, $1/2 + z$

2.
$$\bar{x}$$
, 3/4, z

4.
$$1/2 + x$$
, $1/4$, $1/2 - z$.

The y coordinates in the Fourier map are fixed at some multiple of 1/4. However, the Patterson map does not directly give the position of an atom but only the vector between two atoms. The vectors that arise from these positions are given in Table II. The bromine Patterson peak was located at coordinates $\frac{2.5}{48}$, $\frac{24}{48}$, $\frac{7.2}{30}$. These transformed

Table I. Symmetry relationships of space group Pnma.

Pnma $P 2_1/n 2_1/m 2_1/a$ Orthorhombic mmm No. 62 D_{2h}^{16} Oi. Origin at I iunder of pentions, Mychall notation, ad point symmetry Co-ordinates of equivalent positions Conditions limiting possible reflections General: $x_1y_1z_1^2 = \frac{1}{2} + x_1\frac{1}{2} - y_1\frac{1}{2} = z_1^2 - x_1\frac{1}{2} + y_1z_1^2 - \frac{1}{2} - x_1y_1\frac{1}{2} + z_1^2$ Mrt. No conditions X, y, z; $\frac{1}{2} - x, \frac{1}{2} + y, \frac{1}{2} + z$; $x, \frac{1}{2} - y, z$; $\frac{1}{2} + x, y, \frac{1}{2} - z$. Okt: k+1-2n AOI: No conditions AkO: h-2n h00: (h-2n) 0k0: (k-2n) 00i: (l-2n)Special: as above, plus' $m = x, 1, z; \quad x, 2, 2; \quad 1 - x, 2, 1 + z; \quad 1 + x, 1, 1 - z.$ no extra conditions T 0,0,1; 0,1,1; 1,0,0; 1,1,0. hkt: h+1 2n; k 2n T 0,0.0; 0,1.0; 1,0.1; 1,1.1. Symmetry of special projections (001) $pgm; a' \cdot a/2, b' - b$ (100) cmm; b'-b, c'-c (010) PEE; c'-c, a'-a

Table II. Patterson vectors for bromine in space group Pnma.

	X.1.Z	 x,₃. z .	1-X.3,1+Z	1 +X, 1 , 1-Z
x. 1, z	0	2X1_,2Z	1 +2X,-1 -1 2	-1 ₂ .0,-1 ₂ +2Z
x.₃.z	2 ₹ .1.2₹	o	- <u>1</u> ,0,- <u>1</u> -2Z	- <u>1</u> - 2X <u>1</u> - <u>1</u>
$\frac{1}{2}$ -X, $\frac{3}{4}$, $\frac{1}{2}$ +Z	1-2X 1 · 1 2	1.0.1+2Z	0	2 ▼ .1.2Z
1 + X. 1 . 1 - Z	-1 ,0,1-2Z	1 +2X,-1 . 1 2	2X,- <u>1</u> ,2₹	0

to the Fourier coordinates

$$u = 2\bar{x} = \frac{2.50}{48}$$
 \Longrightarrow $x = \frac{-1.25}{48}$
 $v = \frac{1}{2} = \frac{24}{48}$ \Longrightarrow $y = \frac{1}{4}$
 $w = 2z = \frac{7.2}{30}$ \Longrightarrow $z = \frac{3.6}{30}$.

The Fourier coordinates $2\bar{x}$, 1/2, 2z were chosen to conform with other bromine-containing organic compounds studied in this laboratory in which the bromine atom has a negative x coordinate.

The atomic coordinates of bromine can be derived from these vectors. They, in turn, will be used to phase the electron density (Fourier) map. The Fourier synthesis leads to a map of all atomic positions. The approximate coordinates thus obtained are now rerun to give a first-corrected Fourier map.

Hydrogen atoms cannot usually be placed by this procedure. Often, though, a difference Fourier map can be used to position them. This is obtained by subtracting off all known atomic coordinates. A few peaks of positive density in an otherwise featureless map should remain. These are the hydrogen atom coordinates. If this method fails, there are other indirect means of locating the hydrogens.

Once the first corrected set of atomic coordinates has been obtained from the Fourier map, a process known as refinement is initiated. The ease or difficulty with which this proceeds depends in large measure on how good the

Fourier model is. If the trial structure is poor, then the atom coordinates may converge to a false minimum and a new trial structure has to be formulated. Conversely if the trial structure is good, then the model will converge rapidly to a true minimum.

D. Least-Squares Methods

Least-squares methods attempt to fit the data to a linear equation or a set of linear equations. The success of the least-squares X-ray programs is attributable to the fact that the data set far exceeds the number of parameters to be fit. The "excess" data are needed because of uncertainties in the measurements. The ratio of data points to parameters for a successful structure determination is in the realm of 5 or 10 to 1.

The least-squares routine minimizes the discrepancies between the observed and the calculated structure factor amplitudes:

$$\rho = \sum_{hk\ell} w_{hk\ell} [|F_{obs.hk\ell}| - |kF_{calc.hk\ell}|]^2, \qquad (23)$$

where $w_{hk\ell}$ is a weighting function equal to the inverse of the square of the standard deviation, and k is a scaling factor necessitated by the fact that the data are not on an absolute scale. Here k is treated as another parameter to be varied.

It is not necessary to refine over all the atoms in the unit cell. Only the unique portion of the unit cell, the

asymmetric unit, need be considered in the refinement process. For N atoms in the asymmetric unit, there are (9N + 1) parameters. In addition to the scale factor, there are three positional and six thermal quantities per atom.

The error is minimized by taking the first derivative of R with respect to each variable and setting it equal to zero. This will yield (9N + 1) independent linear equations. In practice there are frequently less than (9N + 1)parameters due to conditions imposed on the position and thermal factors by the space symmetry. Referring to the earlier example of bromomalonamide, it was shown that the coordinates of the bromine, carbon, and hydrogen atoms in the mirror plane are each fixed at 1/4. The space group further requires that two of the thermal parameters for each be fixed at zero. Also, all hydrogen atoms were assigned invariant isotropic thermal parameters. Therefore, instead of the anticipated seventy-three variables there are only forty-nine. This enhances the data-to-variable ratio considerably. Similar considerations hold for other crystal systems.

At the outset of this section it was mentioned that least-squares methods were applicable to linear equations. The structure factor, though, is not linear but transcendental, i.e. a sum of sine and cosine terms. It can be made to approximate a linear equation by expanding in a Taylor series about the parameters. Terms higher than first order

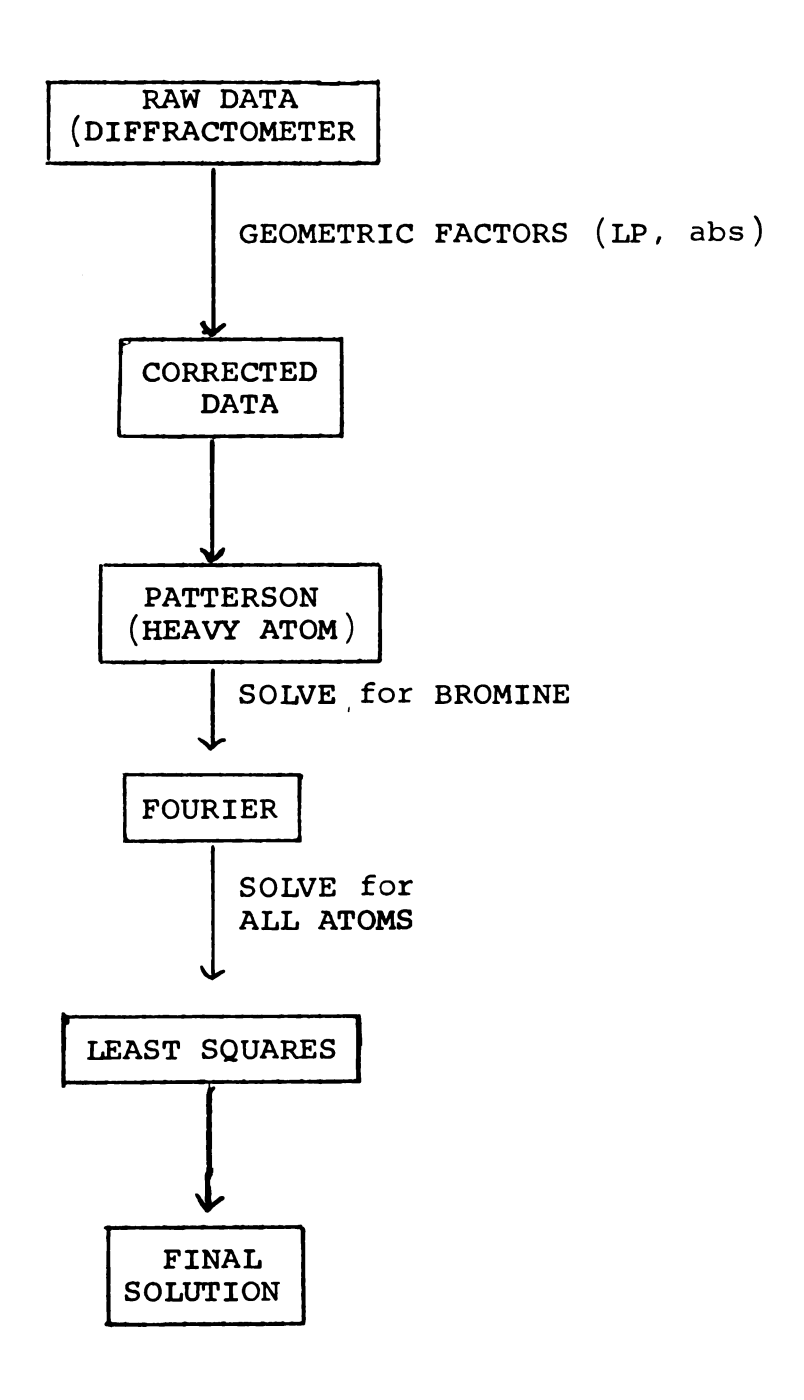
are discarded. This truncation is permissable only if the postulated structure is reasonably close to the correct structure. As the refinement progresses and the standard deviations become smaller, the linear approximation becomes increasingly better because the higher order terms, which have been discarded, approach zero.

One measure of the correctness of the structure is the residual, R. For diffractometer data, the R value should be in the range of 3 to 9 percent.

The reasonableness of the bond distances and angles, and the molecular configuration is another criterion. The refinement proceeds in the following manner:

- 1) temperature factors are isotropic and constant,
- 2) temperature factors are isotropic and variable,
- 3) temperature factors are anisotropic and variable. The scale factor, k, and positional parameters are varied throughout the entire procedure.

Table III. Experimental sequence for the bromomalonamide structure determination



V. EXPERIMENTAL PROCEDURES

A. Preparation of Bromomalonamide

Bromomalonamide 18 was prepared by the slow addition of bromine to a chilled solution of formic acid and malonamide. The mixture was allowed to stand for several hours while it was stirred. The white precipitate which resulted was filtered and washed with chloroform, followed by cold water. It was then recrystallized from ethanol. A further yield was obtained by evaporation of the supernatant liquid under reduced pressure. The melting point of the product was 178-180°.

Analysis	% C	%н	%n	%Br	
Expected	19.89	2.76	15.47	44.19	_
Reported	20.02	2.48	15.53	43.99	

Deuterated crystals were obtained by exchanging bromomalonamide with D_2O three times. Crystals were grown from both CH_3OD and D_2O . The morphology was the same in either case; colorless crystals elongated along the baxis. NMR spectra indicated that the exchange was nearly complete since no proton peaks were observable. The final product of the deuteration process was $(D_2NCO)_2CDBr$.

B. Selection and Alignment of Crystals

Generally, the crystals selected for X-ray diffraction work will range in size from 0.2 to 0.5 mm on an edge. The actual dimensions are checked on a calibrated binocular microscope. A crystal that is too large can be cut to the required size and shape with a razor blade. Since this study of bromomalonamide included both an X-ray diffraction portion and an electron spin resonance portion, the crystal morphology was carefully examined so that the axes identified from the crystallographic work could subsequently be used for the alignment of the crystals for ESR work. A crystal of bromomalonamide and its axes are shown in Figure 2. The dimensions of the crystal were 0.5 x 0.30 x 0.32 mm.

A further examination of the crystal under a polarizing microscope is required to determine whether the crystal is twinned and to aid in the initial alignment of the crystal in the X-ray beam. The crystal is then fastened with glue onto a glass filament. The glue, usually Amberol, Duco cement or Canada balsam, is allowed to dry overnight to ensure that the crystal is firmly in place. The glass filament is attached to a goniometer head, a device which facilitates the alignment and centering of the crystal. The goniometer head consists of two movable arcs which are calibrated in degrees and are located 90° apart. Each arc allows corrections of up to 20° with an accuracy of about a half a degree.

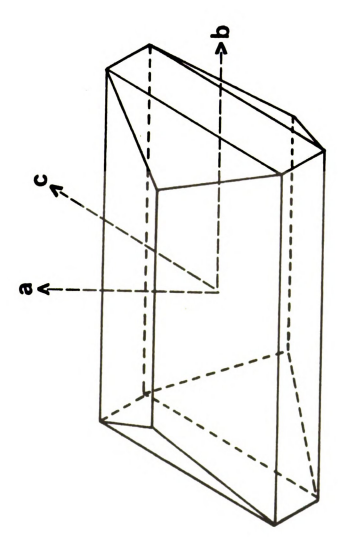


Figure 2. Crystal axes of bromomalonamide.

An excellent description of the goniometer head and alignment procedure is given in the book by Glusker and Trueblood. 19

C. Precession Techniques

Crystals of bromomalonamide were oriented in the X-ray beam by the Polaroid precession method. The crystals were mounted on the goniometer head with the b axis coincident with the axis of the glass fiber and the entire setup was placed on a precession camera (Philips Model XRG 3000).

In addition to the corrections allowed by the arcs on the goniometer head, an additional degree of freedom is introduced by the precession camera. The entire goniometer head was permitted to rotate about a 3600 angle in order to locate the crystallographic axes. The alignment of the crystal and the search for symmetry axes were performed simultaneously. Rotations of the spindle axis were made approximately every 30° over a precession angle of from 10 to 15° until the symmetry axes were found. The entire procedure was accomplished in a few hours. Once the axes were located, two zero-level precession photographs were taken (one for each axis) and from these pictures the lengths of the axes were measured. Each picture required an exposure time of about five hours for the zero-levels and each succeeding upper level photograph required more exposure time. With bromomalonamide, Cu K_{α} X-rays (λ = 1.5405 \mathring{A}) were used for the zero levels, with a nickel filter to exclude beta

radiation, and Mo K X-rays (λ = 0.7079 Å) were used for the first and second levels with a niobium filter.

The parameters to be adjusted before taking precession pictures were the film-to-crystal distance, screen-to-crystal distance, screen size and the precession angle. The screen has an annular aperture which permits only a single level to be photographed at a time. The above parameters are interdependent and the adjustments were made with the assistance of a nomogram. A detailed explanation of the precession method is given in a monograph by M. J. Buerger.²⁰

From the zero-level precession photographs the unit cell dimensions a = 9.515 Å, b = 11.265 Å, and c = 5.870 Å were obtained and the symmetry of the unit cell was determined to be orthorhombic. The photographs actually give the reciprocal lattice axes but, since bromomalonamide is orthorhombic; $a^* = 1/a$, $b^* = 1/b$, and $c^* = 1/c$. Similarly the volume of the unit cell is simply the product of the axes; V = 630.54 Å or $630.54 \times 10^{-24} \text{ cm}^3$. This information, together with the molecular weight, is sufficient to calculate the density of the crystal.

$$\rho = \frac{\text{mass}}{\text{volume}} = \frac{(z)(MW)}{(N)(V)}$$
 (24)

where MW is the molecular weight of bromomalonamide, 181 gm mole⁻¹, N is Avogadro's number, 6.02×10^{23} molecules mole⁻¹, V is the volume of the unit cell, 630.54×10^{-24} cm³, and Z is the number of molecules in the unit cell. Z is unknown, but for an organic compound such as

bromomalonamide only three choices were likely, 2, 4, or 8. From ESR data, which were collected concurrently with the X-ray data, the choice of two molecules per unit cell was not possible and eight was not very likely, which left four as the most probable number. The calculated denisty, based on four molecules in the unit cell, was found to be 1.90 gm cm⁻³. The density was determined by another, independent process, the flotation method. A crystal of bromomalonamide was allowed to float in a beaker containing iodomethane (ρ = 2.28 gm cm⁻³), and dichloromethane (ρ = 1.34 gm cm⁻³) was added dropwise until the crystal remained suspended in the mixture. The density of bromomalonamide was determined to be 1.85 gm cm⁻³. This compares favorably with the value obtained from the X-ray data and confirms the assumption that the unit cell contains four molecules.

The upper levels, first and second levels, as well as the zero-level precession pictures were needed in order to assign bromomalonamide to its proper space group. On the basis of systematic absences in the precession photographs, which revealed that for ok! reflections, k + ! was odd and for hko reflections, h was odd, bromomalonamide could be assigned to either space group Pnma (centric) or Pn2₁a (acentric). Since these differ only by a center of symmetry, the ESR data were not able to distinguish between them. The surest way to make a correct choice was to do the complete crystal structure; this showed the space group to be centric and, therefore, Pnma. An explanation of the symbols and a

listing of all 230 space groups is available in Volume I of the International Tables for X-ray Crystallography. 10 The space group Pnma is based on a primitive, orthorhombic There is a twofold screw axis along each edge of the unit cell, a mirror plane perpendicular to the b axis and, of course, a center of symmetry. The other symmetry elements present in the unit cell are an a glide perpendicular to c and an \underline{n} glide perpendicular to the a axis. The \underline{a} glide consists of a mirror in the ab plane followed by a translation of $\frac{a}{2}$, and the <u>n</u> glide consists of a mirror in the bc plane followed by a translation of $(\frac{b}{2} + \frac{c}{2})$. The space group designation also lists eight positions in the unit cell. Since there are only four molecules to assign to these eight positions, there must be half of a molecule per position or $\frac{1}{2}$ molecule in the asymmetric unit. This means that the crystal structure of bromomalonamide entails locating only the $C-C-NH_2$ moeity. The rest of the

contents of the unit cell can be generated by application of the symmetry elements of the Pnma space group.

Diffractometer D.

The intensity data were collected with a Facs-I Picker diffractometer, a fully automated model, using Mo K_{α} radiation. Initially, twelve reflections of moderate intensity were selected at random and processed by a least-squares routine to further refine the lattice parameters obtained

from the precession photographs. The cell dimensions thus refined were a = 9.487(3) Å, b = 11.294(4) Å, c = 5.885(3)A with the standard deviations in parentheses. The Picker diffractometer employed a graphite monochromator, so that only a narrow wavelength reached the crystal, and a scintillation counter to measure the intensities of the diffracted beam. An omega scan of 1.0° with a scan rate of 0.5° min⁻¹ was used to integrate the reflection intensities. Tensecond background counts were measured at the beginning and end of each scan. The background resulted from stray radiation and scattering of the X-ray beam by air and dust. scan range in theta was from 2.5 to 45°. Beyond 45° so few observed reflections were noted that it was not considered worthwhile to extend the scan range. The intensities of three standards were checked every 100 reflections. These were used to determine if crystal decomposition were occurring during the data collection process. No deterioration was indicated from the intensities of the test reflections.

For an orthorhombic system, the unique data are contained within a single octant. In this instance the $\bar{h}k\ell$ octant was chosen and the $hk\ell$ octant was also measured to corroborate the alignment of the crystal in the diffractometer. The intensities from the two octants were judged to be equivalent and thus confirmed our alignment. The automatic attenuator was not in operation when our measurements were made. Consequently, the strongest reflections overloaded the scintillation counter and had to be

redetermined on an individual basis after the remainder of the data had been collected. The attenuation factor had to be calculated manually which meant re-collecting ten reflections with the attenuator in place to establish a value for the attenuation factor. The twenty-four reflections which overloaded the counter were then measured and the same attenuation factor applied. Of the 543 independent reflections collected, 270 had intensities $\geq 3\sigma$ (I) and could be classified as observed; σ (I), the standard deviation of the intensity, is given by:

$$\sigma \ (I) = [\text{counts} + \text{background} + \text{xnet}^2 \times 10^{-3}]^{1/2}, \ (25)$$
 where xnet = (counts - background). The data from the diffractometer was output in two formats--as paper tape which

could be easily converted to computer cards and as teletype printout which provided a printed record of the data.

E. Data Processing

The first step in data processing was to sort out the unobserved data using Equation 25. Then a decision had to be made whether an absorption correction was needed. The sorting procedure, using DATCOR, 21 included two geometric correction effects, the Lorentz-polarization factors.

The optimum thickness of a crystal is given by an equation found in Stout and Jensen:²²

$$t_{opt} = \frac{2}{\mu} \tag{26}$$

where µ, the linear absorption coefficient, is a function of the wavelength of radiation employed. For organic crystals which do not contain a heavy atom, the linear absorption coefficient is usually less than 1 cm $^{-1}$ for Mo K radiation and the optimum crystal thickness is about 2 cm. Absorption effects are therefore negligible or can be accomodated by the scaling factor in the later stages of the refinement. In either event a separate calculation need not be performed for a simple organic compound to correct for absorption effects. The linear absorption coefficient for bromomalonamide, calculated from Equation 2, is 68 cm⁻¹ and the optimum thickness is 0.029 cm or 0.29 mm. The thickness of the crystal used in this study was 0.5 mm; therefore it was decided to perform an absorption correction. Most books recommend that the crystal be ground or shaped into a sphere so that the absorption of radiation by the crystal would be isotropic. This could not be done for bromomalonamide since it was necessary to locate the axes as a function of crystal geometry so that this information could be used for ESR studies. Such information would be lost in the shaping process. A computer program, ABSCOR, 23 which was written for a crystal of specified general shape, was therefore utilized to correct for absorption effects. The transmission factors obtained from this program ranged from 0.19 to 0.34.

The data were now in the appropriate form to obtain the Patterson and Fourier syntheses.

F. Patterson and Fourier Maps

A packing routine (PACK 5)²⁴ produced a list of all intra- and intermolecular contacts within a 4 Å radius of a central molecule of bromomalonamide and also the symmetry elements which generated the contact. The intermolecular contacts between the nitrogen and oxygen atoms were sought. The approximate coordinates of the hydrogens were derived from the nitrogen-to-oxygen distance. There were no voids or gaps within the 4 Å search radius large enough to accomodate a methanol of crystallization. The packing analysis, thus, confirmed the Fourier difference in this respect.

A full-matrix least-squares refinement was carried out in which the scale factor, atomic coordinates and isotropic thermal parameters were varied. In the final two cycles of the least-squares program, anomalous dispersion corrections were introduced for bromine and anisotropic thermal parameters were used for all atoms except hydrogen. The hydrogen atom thermal parameters were kept isotropic and held fixed but the positional parameters were allowed to vary. For 270 observed reflections and 48 variables, the R value for the unit-weighted structure factors converged to $R_1 = 0.029$ and $R_2 = 0.030$ where

$$R_1 = \frac{\sum |F_0| - F_C|}{\sum F_0}$$
 (27)

$$R_{2} = \left[\frac{\sum w(|\mathbf{F_{0}}| - |\mathbf{F_{c}}|)^{2}}{\sum w|\mathbf{F_{0}}^{2}|}\right]^{1/2}.$$
 (28)

The Patterson vector map was generated by program

PATTR²⁵ with the b axis perpendicular to the plane of the page. After the map had been contoured, a search was made for the bromine vector. The magnitude of the bromine vector peak was by far the largest in the map. The symmetry requirements of space group Pnma were such that the bromine atom had to lie in the mirror plane of the molecule which coincided with the mirror plane of the crystal. Positioning the b axis of the Patterson map perpendicular to the plane of the paper meant that the bromine atom was in the plane of the page and along a page edge. From these considerations it can be seen that the bromine vector and consequently the bromine atomic coordinates were readily located.

The Fourier map, phased only by the bromine atomic coordinates, was generated by program $FORO1.^{25}$ A second Fourier synthesis was run using all of the non-hydrogen atom coordinates. This had only a slight effect on the residual value. An attempt was made to find the hydrogen atoms by using a Fourier difference map. In a difference map, the coefficients are $(F_{\rm obs} - F_{\rm calc})$ and the phase angle is that of the trial structure. A positive peak is expected if insufficient electron density is given to an atom or if the coordinates assigned to an atom are incorrect. No positive peaks were found in the Fourier difference map which meant that the hydrogen atoms did not contribute sufficient electron density to the structure to be detected. A packing analysis was then utilized to determine indirectly the

atomic coordinates of the hydrogen atoms.

A phenomenon occasionally encountered among amides is the thermal averaging of the nitrogen and oxygen atomic positions. To check out this possibility in bromomalonamide the thermal and positional parameters of the nitrogen and oxygen atoms were interchanged. The new structure, after two cycles of least-squares refinement, converged to an R₁ of 0.046 with no appreciable change in bond lengths. The thermal factors of the "nitrogen" atom, however, were not positive-definite; this indicated a deficiency of electron density about the "nitrogen" atom. Therefore, it was concluded that no positional averaging of the nitrogen and oxygen atoms is occurring and that these atoms are distinguishable in the bromomalonamide structure. Table IV lists the observed and calculated structure factors.

	402	********
	Ę	252388 - 328255
70	٠	***************************************
nes		
values	F085 FCAL	**************************************
	Ē	
11	×	
<u>ө</u>	ಕ	
e G	FORS FCAL	
mic		~~~~~~~~
ทลเ	1	
110	FORS FCAL	\$345000000000000000000000000000000000000
omo	7085	
bromomalonamide (all	¥	
bro		
	FORS FCAL	
for	ě	
ហ	z -	
Ö	Š	11122 1212 1212 1212 1212 1212 1212 12
factors	\$6	::
	*	• • • • • • • • • • • • • • • • • • • •
H.	.	Mr-480-N4-48-44-48-44-48-44-48-44-48-44-48-44-48-44-48-44-48-44-48-44-48-44-48-44-48-44-48-44-48-44-48-44-48-4
) tu	35.2	Werthill with the state of the
on.	5	#160 #31 #2 # 1 # 1 # 1 # 1 # 1 # 1 # 1 # 1 # 1
structure	r	
р	₹.	2000 2000 2000 2000 2000 2000 2000 200
a te	F085 FC4L	**************************************
culated	,	1
1c1	I	
g	đ,	
	F085 FCAL	
and	¥	
Observed a x 10).		791255331111011011111111111111111111111111
, (FORS FCAL	
10 10	2	-
g ×	*	
	ž	£5523 = 522
IV.	FORS FCAL	
	*	**************************************
Table	: :	
e H	FORS FCAL	
	8	· ?!!!!!!!!!!!!!!!!!!!!!!!!!!!!
	=	

VI. RESULTS AND DISCUSSION

A. Molecular Geometry

A stereographic view of the bromomalonamide molecule is shown in Figure 3. The bond distances, bond angles and standard deviations are listed in Table V. These values are in substantial agreement with those reported for similar diamides and the comparison is summarized in Table VI. C(1) - C(2) bond distance, 1.522 Å, is slightly shorter than the 1.54 Å usually found in aliphatic compounds and lies between the extremes reported for malonamide (1.502 Å) and dichloromalonamide (1.560 $^{\circ}$). The C(2)-N bond, 1.290 $^{\circ}$, is somewhat short for an amide and is about the same length as the comparable bond in malonamide and dichloromalonamide before each was corrected for thermal motions. The bond distances and angles involving hydrogen are less certain that those for the remaining atoms as shown by the standard deviations in Table V. The bond angles in the central carbon, C(1), are close to the tetrahedral value, while the carbonyl carbon, C(2), and the nitrogen atom each have a planar arrangement of the atoms bonded to them. The amide groups are planar within experimental error and C(1) is common to the planes of the amide groups of a given molecule;

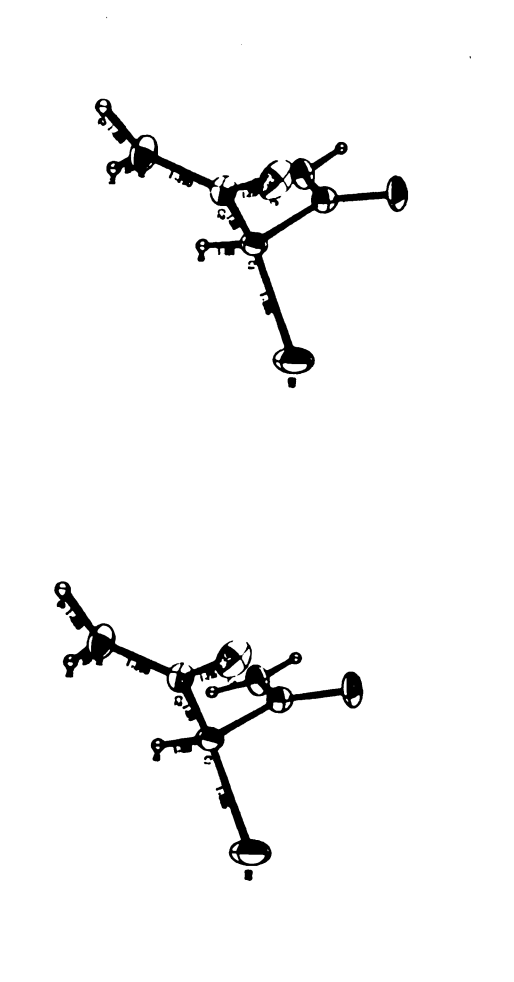


Figure 3. Stereographic view of bromomalonamide.

Table V. Interatomic distances and angles.

Interatomic Dis A	tances	Bond Angles 0			
Br-C(1)	1.954	Br-C(1)-H(3)	113.0(6)		
C(1)-C(2)	1.522(9)	Br-C(1)-C(2)	109.1(5)		
c(2)-o	1.236(7)	C(1)-C(2)-	121.1(6)		
C(2)-N	1.290(5)	C(1)-C(2)-N	112.0(7)		
N-H(1)	0.92(7)	H(1)-N-H(2)	112.0(7)		
N-H(2)	1.11(9)	C(2)-C(1)-C(3)	108.9(8)		
N(1)-H(1)0	2.94	o-c(2)-n	125.0(7)		
N(1)-H(2)0	2.82	C(2)-N-H(1)	123.6(4)		
H(1)o	2.21	C(2)-N-H(2)	124.4(6)		
H(2)O	1.85	ONO	124.8(2)		
BrBr(nonbonded)	4.95	N-HO	164.0(7)		

Table VI. Structural parameters for diamides.

1.243 114.8 119.5		$\begin{pmatrix} av \\ A \end{pmatrix}$ $\begin{pmatrix} av \\ O \end{pmatrix}$	
	.5 125.7	2.945	4
1.253 117.6 119.9	.9 122.6	$2.95 \sim 160^{0} (av)$	-
1.236 113.9 121.1	.1 125.0	2.82 1640	*
1.219 115.9 119.3	.3 124.7	3.006 1620(av)	9
1.238 115.6 122.4	.4 122.0	2.94	က
115.6		5.0	

the angle between these planes is about 109°. One feature in which the molecular geometry of bromomalonamide differs from the remaining diamides^{1,4-6} is the mirror symmetry relating the two amide groups of each molecule.

The molecules are linked together by hydrogen bonds to form a three-dimensional network. Each amide oxygen is linked to hydrogen atoms of two neighboring molecules forming two hydrogen bonds and each molecule is hydrogen-bonded to four neighbors. Along the a axis neighboring molecules form pairs of hydrogen bonds involving both amide groups of both molecules so that 12-membered rings result. Along the c axis neighbors are linked end to end by pairs of hydrogen bonds leading to 8-membered rings. A stereographic representation of this arrangment is shown in Figure 4. Threedimensional hydrogen-bonded networks involving eight- and twelve-membered rings are found in dichloromalonamide, 6 and eight-membered rings in malonamide. 1 Two-dimensional hydrogen-bonded networks with eight-membered rings are found in oxamide4 and, along with eleven-membered rings, in succinamide.⁵ An exceptionally short intermolecular Cl...Cl contact was observed in dichloromalonamide but the intermolecular bromine contacts in bromomalonamide are long.

The configurations of the diamide molecules in the crystals studied vary. In oxamide and succinamide they are completely planar with the oxygen atoms on opposite sides of the molecule. In malonamide the two amide groups are rotated out of the central C-C-C plane by 40° and 65°, respectively,



Figure 4. Stereographic view of the hydrogen bonding of bromomalonamide.

so that the amide groups are nearly perpendicular to each other and, in addition, the amide groups are not quite planar (NH₂ groups $2-14^{\circ}$ out of the C-CON plane). The dichloromalonamide molecules have C_2 symmetry with the NH₂ group only rotated about 5° out of the C-CON plane. Bromomalonamide is unusual in having a mirror plane so that the oxygens are on the same side of the molecule. The intermolecular Br...O distances $(3.15\ \text{Å})$ are slightly shorter than the sum of Van der Waals radii $(3.35\ \text{Å})$ as was found for the Cl...O distance in dichloromalonamide.

It is interesting to consider the possibility of a molecule in which the amide oxygens were on opposite sides as in the other diamides. The molecules would then have C_2 symmetry, apart from the CHBr group, and a space group of lower symmetry Pn2₁a (obtained by discarding the mirror plane of Pnma) would be required. Distance calculations show that the general form of the hydrogen bonding scheme could be retained because the alteration of half of a given molecule (atoms for which 0 < y < b/4) is accompanied by the alteration of the nearest neighbor molecules (-b/4 < y <0). An attempt to refine the structure with this conformation was made but a satisfactory refinement was not obtained. The observed conformation, then, does not appear to be a direct result of the particular hydrogen-bonding pattern but may result from intramolecular interactions such as Br...O. It would be of interest to examine the gas phase or solution dipole moment to determine whether the crystal

conformation is also adopted by the free molecules.

B. Thermal Motions

In the gaseous state free rotation about the C-C and C-N single bonds would be expected but in the solid phase strong intermolecular hydrogen bonding can confer rigidity on the molecules. In bromomalonamide a three-dimensional structure results from the hydrogen bonding network in the ab and ac planes (Figure 4) and this would be expected to be rather rigid.

The thermal motions have been analyzed by the method of Schomaker and Trueblood²⁶ and the TIS (translational, liberational and screw) motions show that the bromomalon-amide molecule is essentially a rigid body and that librational motions are dictated by the hydrogen-bonded network rather than by the bromine atom as would be anticipated for the free molecule. The thermal parameters and atomic co-ordinates of bromomalonamide are given in Table VII.

Tests of the motion included calculations using both mass-weighted Cartesian displacement coordinates (MWCDC) and unit-weighted coordinates of the atoms and these gave equivalent results. The librational and translational tensors are given in Table VIII for both cases. Since the motions are essentially independent of mass, the effect of the hydrogen bonding has been to overcome the influence of mass. For crystals in which the intermolecular interactions are of the Van der Waals type, a mass dependence is observed.

Table VII. Atomic coordinates and thermal parameters for bromomalonamide. The anisotropic thermal parameters are defined as $[-(\beta_{11}h^2+\beta_{22}k^2+\beta_{33}\ell^2+2\beta_{12}hk+2\beta_{13}h\ell+2\beta_{23}k\ell)]$

Atom	x	У	Z	β11	β22	β33	β12	β13	₽ 23
Br	-159	2500	1295	192	141	205	0	13	0
c(1)	873	2 500	-1578	94	78	185	0	-9	0
C(2)	468	1403	-2933	80	64	257	7 5	6	-4
c(3)	468	3 596	-2933	80	64	257	-7 5	6	4
N(1)	1533	806	-3671	71	7 5	415	8	-13	-38
N(2)	1533	4194	-3671	71	75	415	-7	13	38
0(1)	-781	1147	-3271	50	102	424	-21	17	-70
o(2)	-781	3853	-3271	50	102	424	21	17	70
H(1)	2526	983	-3524						
H(2)	1478	246	-4351						
H(3)	2029	2500	-1342						
H(4)	2526	4017	-3524						
н (5)	1478	4754	-4351						

Table VIII. Translation and libration matrices for thermal motions in bromomalonamide.

T Å ²	T Orien	tation	Matrix	r (o) 1	Orient	ation	Matrix		
Unit-Weighted Coordinates									
0.0752	0.386	0.0	-0.922	62.772	0.864	0.0	-0.504		
0.0538	0.0	-1.0	0.0	6.910	0.0	1.0	0.0		
0.0029	-0.922	0.0	-0.386	1.064	0.504	0.0	0.864		
	Mas	s-Weig	hted Coor	dinates (M	IWCDC)				
0.0490	0.0	-1.0	0.0	46.700	0.911	0.0	-0.413		
0.0478	-0.951	0.0	0.308	10.529	0.0	1.0	0.0		
0.0309	-0.308	0.0	-0.951	7.247	0.413	0.0	0.911		

The rigid body approximation for the TLS analysis, on the other hand, assumes that the motion is governed by the intermolecular forces and the mass distribution in the molecule. The concept of an isolated molecule is lost in the presence of the hydrogen-bonding network and, instead, the molecular motion becomes dominated by this polymer-type bonding scheme.

The center of reaction in the molecule lies between the two amino groups, as found using either MWCDC or unit-weighted coordinates. Physically, a line joining these groups could be visualized as a hinge about which oscillations of the molecule may occur. In the free molecule the oscillations would be governed by the moment of inertia of the molecule and would be about the center of mass. In bromomalonamide the motions are, therefore, governed by the hydrogen bonding.

A similar effect was observed in a rigid-body analysis of the thermal motions in trichloroacetic acid, 27 which contains dimers held together by hydrogen bonds. It was shown that there is a libration about the long axis of the dimer so that the molecule moves according to the constraints imposed by the hydrogen bonding. Jönsson and Hamilton used a mass-independent analysis; our recalculation using MWCDC gives slightly improved results and allows us to include hydrogen-atom anisotropic thermal factors as opposed to their enforced neglect in the original treatment. However, our results confirm the conclusion that the molecular motions

(apart from the CCl₃ group rotation) are governed by the hydrogen bonding scheme.

PART II

AN ESR STUDY OF RADICALS IN SINGLE CRYSTALS OF γ -IRRADIATED BROMOMALONAMIDE AND IODOACETAMIDE

I. INTRODUCTION

Electron spin resonance (ESR) spectroscopy is a particularly useful technique for probing the electronic environment of paramagnetic materials. Paramagnetism occurs whenever a substance has one or more unpaired electrons.

Among the transition metal ions and elements, paramagnetism is a commonly encountered phenomenon. Transition metal species can be readily studied by ESR when they are made magnetically dilute by doping into a diamagnetic host crystal.

Organic molecules, on the other hand, are almost always diamagnetic, i.e., all of the electrons are paired. In order for an organic compound to be amenable to ESR techniques, a paramagnetic center has to be induced, usually by ionizing radiation such as X- or γ -rays. The net result, if irradiation is performed on a single crystal or powder, is one or more paramagnetic fragments trapped in the parent compound. The amount of radiation damage is quite small and the paramagnetic center does not require further dilution. Radiation damage in organic compounds usually

results in the formation of a π -electron radical. These radicals are characterized by an unpaired electron which is located in a predominately carbon $2p_z$ orbital, which is perpendicular to the plane of the molecule. Any magnetic nuclei which interact with the unpaired electron are usually situated at or near the nodal plane of the carbon $2p_\pi$ orbital. The magnetic coupling of the electron to such neighboring nuclei is known as hyperfine interaction.

Ionizing radiation applied to organic crystals is always an uncertain procedure in that the damage incurred by the crystal cannot be predicted a priori. However, information available from study of similar compounds can reduce the uncertainty as to the expected radical species.

An ESR study of the radicals in X-irradiated malon-amide, $^{-4}$ $_{12}C(CONH_2)_2$, was among the first single-crystal investigations of organic radicals and as such served as the basis for theoretical calculations, and provided the background for subsequent single-crystal investigations, of other systems. To extend the knowledge of hyperfine inter actions with nuclei other than hydrogen, the $^{\circ}CF(CONH_2)$ and $^{\circ}CF_2CONH_2$ radicals in irradiated difluoromalonamide were examined. Currently γ -irradiated single crystals of chloromalonamide and dichloromalonamide are being investigated and the data available from these studies were helpful in the present work.

The fluorine hyperfine splitting tensors for several π -electron radicals with α -fluorine substituents have been

obtained from single-crystal ESR studies so their geometries and electronic structures are reasonably well known. $^{8-10}$ In the last few years the anisotropic 35 Cl hyperfine interaction tensors have been determined from single-crystal data for the α -chlorine in ·CHClCOOH, 11 ·CFClCONH₂, 12 ·CH₂Cl, 13 (6 Cl₅)₂Ccl¹⁴ and in part, ·CCl₂CONH₂¹⁵ and ·CCl₃. 16 Recently ESR data for the radical ·CHICONH₂ have been reported based on powder spectra. 17 It would, therefore, be of particular interest to have information on a radical, oriented in a single crystal, with an α -bromine, or an α -iodine substituent so that the effects of changing the halogen substituent in a series of π -electron radicals could be evaluated in greater detail.

Unfortunately, carbon radicals with bromine or iodine substituents have proven unusually difficult to study. No reliable values of the isotropic iodine or bromine hyperfine interaction in such a radical appear to be available from solution ESR measurements since such radicals have proved to be quite labile. Attempts to observe the ESR spectra of bromine- and iodine-substituted aliphatic radicals in solution or in an adamantane matrix have failed in this laboratory and some negative results have been reported by other authors. Although there are reports of aromatic radical anions with iodine or bromine substituents no halogen hyperfine splitting was observed; this could mean that a(I) or a(Br) was less than the linewidth or it could result from loss of iodine or bromine. It has been

shown that the latter occurs very readily from anion radicals, usually too rapidly to permit observation of ESR spectra.²¹ The iminoxy radical from 2-bromoacetophenone oxime, although a rather different type of radical, shows a value of a(Br) about as large as a(F) in the analogous fluorine-substituted radical.

Although iodine—and bromine—containing organic radicals are more stable in the solid, the ESR spectra are very complex. Bromine has two isotopes, ⁷⁹Br and ⁸¹Br, each with I = 3/2 but with different magnetic moments and quadrupole moments; there may also be additional hyperfine splitting from other nuclei, site splitting, lines from other radicals and different axis systems for the A(Br), g and e²Qq tensors. These factors, and the resulting extensive overlapping of lines, has hindered ESR work and no complete analysis of single—crystal spectra has so far been reported except for the radical (CH₃)₂S-Br in dimethyl (9-fluorenyl) sulfonium bromide.²² In this radical the odd electron is largely on sulfur so the results are not directly comparable with those for carbon—centered radicals.

A bromine-containing radical was detected in γ-irradiated single crystals of bromoacetic acid but could not be positively identified.²³ The radical ·CF₂Br appears to be present in γ-irradiated single crystals of bromodifluoro-acetamide,²⁴ and the maximum value of the ⁸¹Br hyperfine tensor was found to be 238 G, but a complete analysis was not made. A partial analysis of the bromine tensor in an

excited triplet state of sym-tetrabromobenzene has been carried out. 25 Also, α -bromo radicals have tentatively been identified in five γ -irradiated polycrystalline organic bromides and possible values for some of the tensor components have been listed; 26 interpretation of complex powder ESR spectra is, however, not always unequivocal. Powder data have been used to obtain possible ESR parameters for two radical anions of N-bromo amides and the odd electron is believed to be more or less equally shared between nitrogen and bromine in these. 27

There does not appear to be any previous example of an organic radical exhibiting iodine hyperfine splitting where the ESR spectra could be unambiguously analyzed.²⁸ No isotropic iodine hyperfine interactions for π-electron radicals are available either. A complete analysis of single-crystal spectra of a radical CHICONH₂ is reported here. After this work was completed a communication appeared reporting ESR parameters for the radical CHICONH₂, ¹⁷ data were obtained largely from powder spectra. Agreement between the parameters, where they may be compared, is good considering the difficulties inherent in interpreting powder data. A detailed ESR study of ·CHBr(CONH₂) is also reported here. This radical has been obtained in bromomalonamide γ-irradiated at 77°K and both powder and single-crystal ESR spectra have been analyzed. A second radical, ·CONH₂, is

simultaneously produced but has not been investigated. Interference from the lines of the latter radical has, however, been greatly reduced by employing ${\rm CDBr}({\rm COND_2})_2$ in the present work.

II. LITERATURE SURVEY

Numerous textbooks, monographs and reviews are available which discuss in detail the theoretical and experimental aspects of electron spin resonance spectroscopy. A review by J. R. Morton²⁹ gives a comprehensive survey of the field of ESR from its inception until the time of the article in 1964. Morton presents a primarily qualitative discussion of the developments in the field and provides a complete set of literature references at the conclusion of the article.

A more recent article by A. Carrington and H. C. Longuet-Higgins³⁰ stresses the theoretical concepts of an ESR experiment with several sample calculations on transition metal ions. Carrington³¹ has also authored a review featuring the ESR of aromatic molecules in solution.

Books by Carrington and McLachlan, ³² Wertz and Bolton, ³³ and Ayscough ³⁴ provide a satisfactory introduction to theoretical as well as experimental considerations involved in a magnetic resonance experiment. More advanced treatment of the theory is presented in books by Slichter, ³⁵ and by Poole and Farach. ³⁶ All of the pertinent quantum mechanical equations are gathered in a rather encyclopedic text by

Abragam and Bleaney.³⁷ These authors make little effort, however, to present a rigorous derivation of the equations.

Treatments of the experimental aspects of ESR including intrument design and technology are provided in books by Poole³⁸ and Alger.³⁹ The book by Alger has an extensive section on low-temperature techniques, a topic that is becoming of increasing importance to the experimentalist.

III. THE ESR EXPERIMENT

The unpaired electron in a paramagnetic species has associated with it the property of spin. The combination of spin and charge result in a net magnetic moment. The relationship between the spin angular momentum, \vec{s} , and the magnetic moment, $\vec{\mu}_e$, is expressed by Equation 1, where g_e and β_e are proportionality constants:

$$\bar{\mu}_{e}^{\rightarrow} = -g_{e} \beta_{e} \bar{s}^{\rightarrow} \tag{1}$$

In a standard electron magnetic resonance experiment, the paramagnetic sample is placed in a magnetic field, $\overline{H}^{>}$. The interaction of the field with the magnetic moment is then:

$$\bar{E}^{\prime} = \bar{\mu}_{e}^{\prime} \cdot \bar{H}^{\prime} = -g_{e}\beta_{e} \bar{S}^{\prime} \cdot \bar{H}^{\prime}$$
 (2)

For a magnetic field applied in the z direction, Equation 2 reduces to the form:

$$E = -g_e \beta_e HS_z$$
 (3)

where $S_{\mathbf{z}}$ is the component of spin angular momentum in the \mathbf{z} direction.

There are several energy levels which correspond to the (2S + 1) orientations (each designated m_S) which the

spin vector will have in a magnetic field. For a single electron with S=1/2, there are only two possible orientations, $m_S=+1/2$ or $m_S=-1/2$. This is referred to as a spin multiplicity of 2 or a doublet state.

An oscillating field with a frequency, v, is applied perpendicular to the static field. This microwave frequency is kept constant while the magnetic field is swept until the resonance conditions are satisfied. At this point, a transition is induced between the two energy states of the electron. Because the magnetic field is swept during an ESR experiment, hyperfine splitting values are commonly reported in units of gauss. The resonance equation is

$$\Delta E = h v = -g_e \beta_e H \qquad (4)$$

where, h = Planck's constant = 6.62×10^{-27} erg - sec, v = microwave frequency in units of megahertz or

g = Landé g factor (unitless),

gigahertz,

 β_e = Bohr magneton = 9.27 x 10^{-21} erg gauss⁻¹,

H = magnetic field in units of gauss.

Electron spin resonance spectra are characterized by three types of parameters: A, Q, and g_e, which provide information about the environment of the unpaired electron. All are tensors of the second rank and can be represented as symmetric 3 x 3 matrices. By a suitable rotation of coordinates, each matrix can be put into the more familiar and convenient diagonal form, then elements along the digonal

of each matrix are known as the principal values of the tensor. Thus, for the A tensor:

$$\bar{\bar{A}}^{\, >} = \begin{pmatrix} A_{xx} & A_{xy} & A_{xz} \\ A_{yx} & A_{yy} & A_{yz} \\ A_{zx} & A_{zy} & A_{zz} \end{pmatrix} \implies \begin{pmatrix} A_{xx} & 0 & 0 \\ 0 & A_{yy} & 0 \\ 0 & 0 & A_{zz} \end{pmatrix} (5)$$

IV. THEORY

A. Spin Hamiltonian

Paramagentic resonance phenomena are usually explained on the basis of quantum theory if information regarding line positions and transition probabilities is desired. Since the magnetic resonance experiment provides many of the parameters used in the energy evaluation, the quantum mechanical treatment is semi-empirical. In order to interpret a magnetic resonance spectrum, it is first necessary to postulate a spin hamiltonian, \mathcal{K}_{\bullet} . This quantity operates on the appropriate wavefunction, ψ , to give the energy states. The proper wavefunctions are derived from combinations of nuclear and electron spin functions.

$$\mathcal{K}\psi_{e}\psi_{n} = E\psi_{e}\psi_{n} \tag{6}$$

The exact form of the Hamiltonian will vary according to the complexity of the system under consideration. The experimentalist must decide which terms in the Hamiltonian give an adequate description of the expected interactions. A general Hamiltonian suitable for the systems treated in this dissertation is given by Equation 7:

 $\mathcal{K} = \mathcal{H}_{electron Zeeman} + \mathcal{H}_{nuclear hyperfine} + \mathcal{H}_{quadrupole} + \mathcal{H}_{nuclear Zeeman}.$ (7)

The Hamiltonian has been separated into several terms to facilitate the ensuing discussion. The terms are listed in order of decreasing magnitude of effect.

- 1) $\mathcal{K}_{electron\ Zeeman} = \beta_e\ \bar{s}^>\cdot \bar{g}^>\cdot \bar{H}^>$. The interaction of the spin angular momentum with the magnetic field is known as the electron Zeeman effect. For organic radicals this is by far the strongest interaction. Since g varies but little from the free spin value of 2.0023 for organic radicals, it can be treated as a scalar quantity and the Hamiltonian simplifies to $g_e\beta_e\ \bar{s}^>\cdot \bar{H}^>$ where g_e and β_e are constants. When a heavy atom such as bromine or iodine is present, the possibility of spin-orbit coupling exists and G must be treated as a tensor quantity. The g tensor is an experimental parameter and is referred to as the spin-orbit coupling term, the Lande g factor, or the spectroscopic splitting term.
- 2) $\mathcal{K}_{\text{nuclear hyperfine}} = \bar{S}^{>} \cdot \bar{A}^{>} \cdot \bar{I}^{>}$. This portion of the Hamiltonian represents the interaction of the magnetic moment of the nucleus and the magnetic field due to the spin and orbital moments of the odd electron. A, like g in the preceding paragraph, is a second rank tensor and is known as the hyperfine splitting tensor and also must be evaluated experimentally. $\bar{S}^{>}$ and $\bar{I}^{>}$ are the electron and

nuclear magnetic moments, respectively. The A tensor can be further subdivided into an isotropic, or non-directional, portion and an anisotropic, or directional, portion. It is frequently written as such to reflect this fact:

$$\vec{s}^* \cdot \vec{A}^* \cdot \vec{r}^* = \vec{s}^* \cdot \vec{r}^* - g_e \beta_e g_n \beta_n \left[\frac{\vec{r}^* \cdot \vec{s}^*}{r^3} - \frac{3(\vec{r}^* \cdot \vec{r}^*)(\vec{s}^* \cdot \vec{r}^*)}{r^5} \right]$$
(8)

The isotropic coupling constant is given by a scalar, a, where

$$a = \frac{8 \pi}{3} g_e \beta_e g_n \beta_n \delta(r)$$
 (9)

The presence of a Dirac delta function, $\delta(r)$, in Equation 9 enables a physical interpretation to be given to a. The Dirac delta function has a finite value only when r=0. This means that the isotropic coupling constant exists if the unpaired electron is at the nucleus. Since s orbitals have no node at the nucleus, a can be related to the s character of the unpaired electron. The isotropic coupling constant is obtained from the trace of the diagonalized hyperfine tensor, i.e.

$$a = \frac{1}{3} (A_{xx} + A_{yy} + A_{zz})$$
 (10)

When the isotropic contribution to the hyperfine splitting is subtracted from each of the diagonal elements of the matrix, the anisotropic portion remains. This is a traceless tensor, i.e. the diagonals sum to zero. The notation for the anisotropic component is B.

where $B_{xx} + B_{yy} + B_{zz} = 0$.

The dipolar or anisotropic hyperfine parameter, B, is inversely proportional to the distance, r^{-3} , between the unpaired electron and the magnetic nucleus. This term is sometimes written in another form to emphasize its direction dependence:

$$B = g_e \beta_e g_n \beta_n \left\langle \frac{1 - 3 \cos^2 \theta}{r^3} \right\rangle_{av}$$
 (12)

where θ is the angle between a principal axis of the tensor and the line connecting the nucleus with the unpaired electron. For an electron in an sorbital, Equation 12 averages to 0. Therefore, the anisotropic term can be related to the p and d character of the odd electron. In the solid state only the combined effects of these two quantities, i.e. isotropic and anisotropic terms, can be measured.

3) $\mathcal{H}_{\text{quadrupole}} = Q'[I_Z^2 - \frac{I}{3}(I+1)]$. A third tensor quantity which is present only for nuclei with nuclear spin $I \geq 1$, is the quadrupole term. Like the g and A tensors, it can be represented as a 3 x 3 matrix. Since the quadrupole tensor is traceless, only two of the diagonal

elements of the matrix are necessary to specify it. The nuclear electric quadrupole moment, Q, is a measure of the non-spherical charge distribution within the nucleus. The quadrupole coupling constant is electrostatic in nature and arises from the interaction of the nuclear quadrupole moment with the field gradient of the electrons at the nucleus. The Q' term in the Hamiltonian is

Q' =
$$\frac{3e^2 Q}{4I(2I-1)} \frac{\partial^2 V}{\partial z^2} = \frac{3e^2 Q q_{zz}}{4I(2I-1)}$$
, (13)

where e is the electronic charge, Q is the quadrupole moment and q_{zz} is the gradient of the electric field at the nucleus. The q_{zz} term is equal to the second derivative of the electrostatic potential, V, with respect to the molecular axis coordinate, z. The quadrupole coupling constant is contained within the Q' parameter and is equal to e^2Qq_{zz} . The magnitude of the coupling constant is usually reported in units of megahertz.

The presence of a nucleus with a quadrupole moment can make spectra appear complicated especially if the quadrupole and hyperfine coupling are of the same order of magnitude. The magnetic and electrostatic interactions each attempt to orient the nucleus about its own axis. The principal effects of this are line broadening, irregular line spacing, and the presence of "forbidden" transitions. The normal "allowed" transitions correspond to $m_s = \pm 1$, $m_I = 0$ while forbidden lines have $m_s = \pm 1$, $m_I = \pm 1$, ± 2 . Occasionally

the "forbidden" lines may be more intense than the "allowed" lines, making interpretation of the spectrum difficult.

4) $\mathcal{H}_{nuclear\ Zeeman} = g_n \beta_n\ \vec{l}^*\cdot \vec{H}^*$. This is the nuclear Zeeman component of the Hamiltonian and represents the direct action of the magnetic field at the nucleus. It is often small and in many instances is omitted from the complete Hamiltonian. It is included here for the sake of completeness.

B. Approximate Solutions

Since the equations that result from use of the full Hamiltonian in Equation 7 are rather formidable, it is often necessary to resort to approximate methods of solution. The perturbation method is one such approach that has been successfully applied. If the strongest interaction differs by one or two orders of magnitude from the remainder of the terms, then perturbation theory is applicable. In a magnetic resonance experiment, the largest term is the electron Zeeman interaction. Since the magnetic field strength is about 3000 gauss while the hyperfine interaction for a proton usually does not exceed 35 gauss, the perturbation approximation is clearly valid for organic radicals. However, if the organic radical contains bromine or iodine, the maximum hyperfine splitting is nearly 300 gauss. The perturbation treatment can still be utilized but higher-order correction terms have to be considered.

The Hamiltonian is separated into $\mathcal{K}^{(0)}$ for the electron Zeeman term and $\mathcal{K}^{(1)}$ for the remaining interactions. The Zeeman energy is obtained and the other terms are added as small corrections or perturbations.

The necessary equations are given below:

$$|\psi_{i}\rangle = |i\rangle - \{\sum_{i\neq j} \frac{\langle i|\mathcal{K}^{(1)}|j\rangle}{e_{i}-e_{j}}\}|i\rangle$$
 (14)

$$E_{i} = e_{i} - \langle i | \mathcal{K}^{(1)} | i \rangle - \sum_{i \neq j} \frac{\langle i | \mathcal{K}^{(1)} | j \rangle \langle j | \mathcal{K}^{(1)} | i \rangle}{e_{i} - e_{j}}$$
(15)

The perturbation equations have been solved by Bleaney, 40 subject to the conditions that the system have axial or near axial symmetry and that the quadrupole interaction is smaller than the hyperfine term.

The first-order energy levels calculated by Bleaney are

$$E(m_S, m_I) = g\beta_e Hm_S + Km_S m_I + \frac{Q'}{2} [m_I^2 - \frac{I}{3} (I + 1)]$$
 (16)

$$(\frac{3 A^2 g_{\parallel}^2 \cos^2 \theta}{K^2 g^2} - 1) - g_n \beta_n Hm_{\text{I}} (\frac{A g_{\parallel} \cos^2 \theta + B g_{\text{L}} \sin^2 \theta}{K g}),$$

where

- $\boldsymbol{\theta}$ is the angle between the external field and the z axis,
- g_{μ} is the component of the g tensor in the z direction,
- g is the component of the g tensor in the x or y direction,

A is the component of the hyperfine tensor in the z direction,

B is the component of the hyperfine tensor in the x or y direction,

$$K = g^{-1}[A^2 g_{\parallel}^2 \cos^2 \theta + Bg_{\perp}^2 \sin^2 \theta]^{1/2}$$
, and (17)

$$g^{2} = g_{\parallel}^{2} \cos^{2}\theta + g_{\parallel}^{2} \sin^{2}\theta. \tag{18}$$

The energy difference between two energy levels is then $\Delta E = h \nu = g \beta_e H + K m_I$ for the transition $(m_S, m_I) \rightarrow (m_S-1, m_I)$. For the spin system S = 1/2, I = 3/2, the first-order equations predict (2I + 1) or four equally-spaced and equally intense lines. The quadrupole term has the effect of shifting the energy levels but this cannot be detected experimentally because each level is shifted the same amount. When the energy differences are considered in Equation , the quadrupole term is seen to vanish in this first-order treatment.

The expression for the energy levels carried out to second order is:

$$- m_{I} \left(\frac{q_{\parallel} q_{\perp}^{AB}}{g^{2} K^{2}} \right)^{2} \frac{Q^{2} \sin^{2} 2\theta}{8Km_{S}} (8m_{I}^{2} + 1 - 4I(I + 1))$$

$$- m_{I} \left(\frac{q_{\perp}^{B}}{gK} \right)^{4} \frac{Q^{2} \sin^{4} \theta}{8Km_{S}} (2I(I + 1) - 2m_{I}^{2} - 1).$$
(19)

The energy of the transition $E(m_S, m_I) \rightarrow (E(m_S-1, m_I))$ is:

$$\Delta E = hv = g\beta_{e} H + Km_{I} + \left|\frac{A^{2} + K^{2}}{4K^{2}}\right| \frac{B^{2}}{g\beta_{e}H} (I(I+1) - m_{I}^{2})$$

$$+ m_{I}^{2} \frac{(A^{2} - B^{2})^{2}}{8K^{2}g\beta_{e}H} \left(\frac{g_{\parallel} g_{\parallel}}{g^{2}}\right)^{2} \sin^{2} 2\theta$$

$$- m_{I} \left(\frac{g_{\parallel} g_{\parallel} AB}{g^{2}K^{2}}\right)^{2} \frac{Q^{(2)} \sin^{2} 2\theta}{8Km_{S}(m_{S} - 1)} (8m_{I}^{2} + 1 - 4I(I+1))$$

$$- m_{I} \left(\frac{g_{\parallel} B}{gK}\right)^{4} \left(\frac{Q^{(2)} \sin^{4} \theta}{8Km_{S}(m_{S} - 1)}\right) (2I(I+1) - 2m_{I}^{2} - 1).$$

Second-order corrections are obtained by including the off-diagonal elements of the Hamiltonian matrix, which were neglected in the first-order approximation. The off-diagonal elements of the matrix mix the $\mbox{m}_{\mbox{\sc I}}$ and $\mbox{m}_{\mbox{\sc S}}$ wavefunctions. Lines involving transitions corresponding to $\Delta\mbox{m}_{\mbox{\sc I}}=\pm 1$ will now appear in the spectrum. The intensity of these "forbidden" lines is usually weak and is borrowed from that of the "allowed" lines so that as the intensity of the "forbidden" lines increases that of the "allowed" lines decreases.

The $m_{\tilde{I}}^2$ terms which appear in the second-order equation are responsible for the unsymmetrical appearance of the ESR spectrum. Separations between lines either increase or decrease rather than remaining uniform as the spectrum is scanned. The portions of the second-order equations which involve $m_{\tilde{I}}^2$ are field dependent and, in a sufficiently strong magnetic field, the second-order effects described above will disappear and a simple first-order treatment of the spectrum will suffice.

The quadrupole terms which disappeared in the first-order approximation are quite important when the second-order corrections are considered. Terms in $m_{\rm I}^3$ will cause the line spacings to be unequal, but symmetrical about the center of the spectrum. Quadrupole interactions will give rise to "forbidden" transitions corresponding to changes of $\Delta m_{\rm I} = \pm 1$, ± 2 in the nuclear magnetic quantum number. The intensities of these lines will depend on the ratio of Q to B.

Since quadrupole terms are independent of the magnetic field strength, the effects of a quadrupole moment will not vanish at high fields whereas terms involving $\[mathbb{m}^2_I\]$ will diminish in importance. This provides a convenient means of distinguishing between second-order and quadrupole effects.

Figure 1 is an energy level diagram with the expected features for a) first-order, and b) second-order, approximations for a system with S = 1/2 and I = 3/2. The

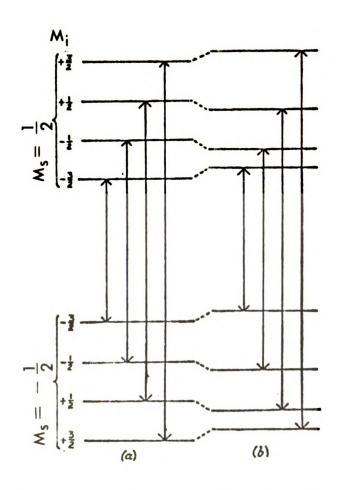


Figure 1. a) First-order energy levels and allowed transitions;

b) second-order energy levels and allowed transitions. reason for the inversion of the nuclear energy levels between $m_S^2 = -1/2$ and $m_S^2 = +1/2$ is that the field at the nucleus reverses during the course of a transition.

The second-order equations reduce to a particularly simple form when the magnetic field is situated along the parallel or perpendicular principal axes.

With the magnetic field along the parallel orientations, θ -> 0^{0} , K -> A, g -> g_{||} and

$$hv = g_{\parallel} \beta_e^H + Am_{\parallel} + \frac{B^2}{2g_{\parallel}\beta_e^{H_{\parallel}}}[I(I + 1) - m_{\parallel}^2].$$
 (21)

With the magnetic field along the perpendicular orientation, $\theta \to 90^{\circ}$, K \to B, g \to g and

$$h\nu = g_{\underline{I}} \beta_{e}H + Bm_{\underline{I}} + (\frac{A^{2} + B^{2}}{4g_{\underline{I}}\beta_{e}H_{\underline{I}}})[\underline{I}(\underline{I} + 1) - m_{\underline{I}}^{2}] - \frac{m_{\underline{I}}Q^{2}}{2B}$$

$$[2\underline{I}(\underline{I} + 1) - 2m_{\underline{I}}^{2} - 1]. \qquad (22)$$

These equations are in a form adaptable to computerization. This is especially desirable for powder spectra, the major features of which consist of contributions from the parallel and perpendicular orientations. A, B, g, g and Q' are parameters to be fit to the line positions given by H_{\parallel} and H_{\parallel} with ν fixed.

Some interesting predications can be made from Equations 21 and 22. The quadrupole interactions completely disappear in the parallel direction. The second-order effects are more pronounced in the perpendicular orientation, where the ratio of the hyperfine terms to the magnetic field

strength is $(\frac{A^2+B^2}{H})$, than in the parallel orientation where this ratio is $\frac{B^2}{H}$. These observations can be quickly checked from the powder spectrum if the features are well-resolved.

V. TECHNIQUES

Electron spin resonance spectra have been recorded of solid, liquid and gaseous samples. Gases are infrequently encountered and will not be considered here. Varying amounts of information are obtained from a spin resonance experiment depending on the form of the sample.

A. Single-Crystal Spectra

In general the greatest amount of information may be extracted from analysis of single-crystal data. The radical is oriented in the host matrix and obeys the same symmetry relationships as the undamaged crystal. If X-ray diffraction data are available, they can provide information on the orientation of the radical species within the crystal and thus facilitate the choice of axes to be used. With a knowledge of the space symmetry and the number of molecules in the unit cell of a compound, the number of magnetically inequivalent sites (site splitting) to be expected for a given orientation of the radical with respect to the magnetic field can be determined. Usually the crystallographic axes are chosen for aligning the crystal in the magnetic field to take advantage of crystal symmetry, and to minimize site splitting. In the event that diffraction data are

unavailable, the crystal is aligned with respect to external features. Three mutually orthogonal axes are selected and rotations are made about each in turn. Spectra are recorded every 5 to 10 degrees, or more often according to the complexity of the radical system. From these rotations the direction cosines, which relate the laboratory axes to the principal axes, and the A, g and Q tensors are obtained.

B. Powder Spectra

Polycrystalline materials and glassy substances give spectra which are an average of all orientations of the radical in the magnetic field. One spectrum contains all of the information that is available from a single-crystal analysis except for the direction cosines. A bewildering array of overlapping lines is frequently encountered and choosing the correct lines is difficult. This makes the interpretation of powder spectra hazardous from the standpoint of assigning transitions correctly. Still, since so much information is available from a single spectrum, it is tempting to try to sort out the various parameters. Consequently, many computer programs have been written to aid in this task.41-43 In the case of radical systems with axial symmetry $(A_{xx} = A_{yy} \neq A_{zz})$ and large anisotropies g and A, some and possibly all of the components of the tensors may be resolved. This is especially true if the spectra are recorded at two different microwave

frequencies. X-band at 9 gigahertz and Q-band at 35 gigahertz are two frequencies routinely employed in ESR experiments. The higher frequency has the further advantage of reducing second-order effects.

C. Solution Spectra

Solution spectra are capable of giving only isotropic values of q and A. Because of Brownian motions, the molecules reorient so rapidly that the dipole and quadrupole interactions are averaged to zero. The absence of these interactions has the additional effect of narrowing the spectral lines. Therefore, solution spectra are capable of giving very accurate values for the isotropic components of the hyperfine and g tensors. Until recently, flow systems were the most common means of generating organic radicals in liquid solutions but these have the disadvantage of requiring large quantities of materials. The photolysis method, 44 which has largely supplanted flow methods, eliminates the waste inherent in the flow system. In a typical photolysis experiment less than 0.5 gm of the organic compound is used. A solution of di-tert-butylperoxide, Me₃COOCMe₃, and the organic substrate are placed in a quartz tube and thoroughly degassed. The tube is placed in the cavity of the spectrometer and subjected to ultraviolet radiation. Radicals are formed within five minutes from the inception of the radiation and are stable for several hours. The reaction sequence is as follows:

Another recent development is the use of solid solutions to obtain isotropic spectra. A mixture of an organic solid or liquid and a host matrix such as adamantane 46 are mixed and the mixture sublimed. The solid solution that results is irradiated with X- or γ -rays. The radical formed in this manner gives an isotropic spectrum indicating that it undergoes free rotation within the host matrix. This procedure is applicable to small molecules containing less than eight heavy atoms since the organic species must displace an adamantane molecule from the lattice.

IV. HYPERFINE SPLITTING

There has been a large collection of data amassed from ESR studies of radiation-damaged organic compounds. Initially, the choice of compounds was limited to the simpler amino acids, amides and carboxylic acids. These substances were readily available, easily crystallized and of biological significance. More recently, interest has been extended to those organic compounds containing one or more halogen atoms. Hyperfine interactions with hydrogen, deuterium, nitrogen and to a lesser degree fluorine and chlorine have now been examined. Tables of hyperfine values for these atoms in representative compounds are provided in the following pages.

A. α -Proton Coupling

An α -proton (I = $\frac{1}{2}$) is one which is directly attached to the atom on which the unpaired electron is predominately located, e.g., $\mathring{\mathbf{C}}$ -H. Both the magnitude and sign of the α -proton coupling value have been theoretically derived and experimentally verified. A semi-empirical equation has been derived by H. M. McConnell⁴⁷ which relates the isotropic portion of the hyperfine tensor to the spin density on the central carbon atoms. The relationship, developed

for a π -electron radical, is

$$a_{H} = Q_{C-H}^{H} \rho_{\pi}(C), \qquad (24)$$

where $\rho_\pi({\tt C}\,)$ is the $\pi\text{-electron}$ spin density on the central carbon atom, $a_{_{\mathbf{H}}}$ is the isotropic hyperfine splitting interaction, the exact value of which is obtained experimentally and ranges from -20 to -24 gauss; Q_{C-H}^{H} is a spin polarization term which has been shown theoretically to have a value of about -23.6 gauss. The spin polarization notation used by McConnell is defined as follows: (1) The superscript (H) indicates the nucleus under consideration. (2) The subscript (C-H) indicates the bond involved, with the first letter of the subscript (C) designating the atom on which the π electron is localized. McConnell's equation is quite general and has been found applicable to a variety of cases. The fact that experimental values for the spin polarization term vary so markedly from the theoretical value is a troublesome feature of this equation. More reliable estimates of Q_{C-H} for a series of substituted alkyl radicals have been presented in a paper by Fischer. 48 The Q_{C-H}^H term is not treated as a unique constant but as a parameter which depends on the $\sigma-\pi$ interaction and reflects inductive and other effects which will change the magnitude of the $\sigma-\pi$ interaction.

The mechanism of the isotropic hyperfine interaction has been treated by a number of authors. 49,50 Valence bond as well as molecular orbital treatments were used and each

gives the same result: the unpaired spin density at the α proton is due to a spin polarization effect. This is pictured for a C-H fragment in Figure 2. The odd electron is located in a carbon $2p\pi$ orbital which is perpendicular to the C-H sigma bond. There are two possibilities for the electron in the carbon sigma orbital. It can have its spin aligned parallel with the odd electron (Figure 2-A) or anti-parallel with the odd electron (Figure 2-B). The former is slightly preferred energetically because an exchange interaction is possible. According to Hund's rule, this would create a slight excess of spin down (beta spin) electrons at the hydrogen nucleus, leading to a negative sign for the coupling constant. The spin polarization effect is quite small as can be seen from the fact that a free hydrogen atom has a hyperfine value of 508 gauss while the value for an α proton is about 20 gauss.

B. β -Proton Coupling

 β -Hydrogens are attached to the atom adjacent to the carbon containing the odd electron, \dot{C} -C- H_{β} . Since β -protons are located rather far from the unpaired electron in a π radical, it is expected that the dipolar interactions, which vary as r^{-3} , should be very small or negligible, making β -proton interactions essentially isotropic. An expression analogous to the one derived for α protons can be obtained:

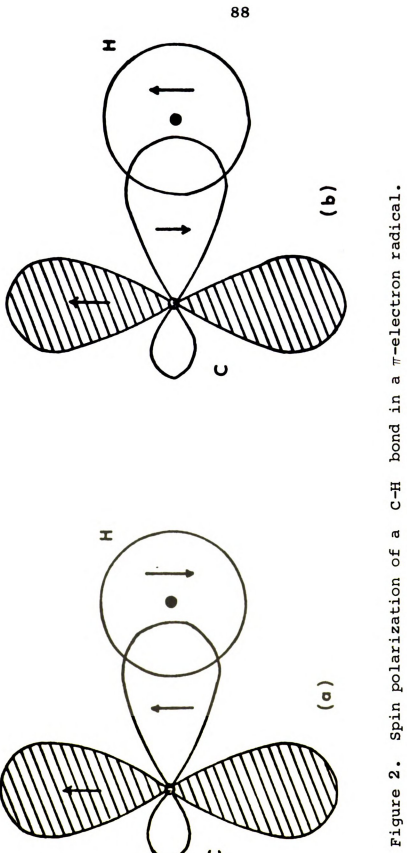


Table I. Representative α -proton hyperfine interactions.

Radical	aiso (gauss)	B _{xx} (gauss)	B yy (gauss)	B _{zz} (gauss)	Ref.
HC(COOH)2	-21.4	11.1	1.4	-10.3	51
$HC\left(CONH_2\right)_2$	-21.2	11.0	0.1	-10.7	1
носнсоон	-20.3	9.6	0.7	-10.3	52
CH ₃	-22.3	-0.2	0.4	- 0.2	53
HOOCCHCH ₂ COOH	-20.3	10.3	0.7	-10.7	54
СН3СНСООН	-21.5	13.0	-2.7	-10.3	55

Table II. Representative β -proton hyperfine interactions.

Radical	a iso (gauss)	B xx (gauss)	B yy (gauss)	B _{zz} (gauss)	Ref.
(CH ₃) ₂ CCONH ₂	21.7	1.0	-0.1	-0.9	56
CH ₃ CHCONH ₂	21.0-25.0				56
$(CH_3)_2CCOOH$	23.4	1.3	-0.4	-0.9	57
CH ₃ CHCOOH	22.3-28.1				55
HOOCCHCH ₂ COOH	28.9				58
он ноос-сн-с-соон он он	10.0	7.8	0.3	-2.1	54

$$a_{H} = Q_{C-C-H}^{H} \rho_{\pi}(C) \cos^{2} \theta \qquad (25)$$

where a_H is the isotropic value for the β proton obtained experimentally, Q_{C-C-H} is a proportionality parameter, ρ (C) is the spin density in the carbon π -orbital, and θ is the dihedral angle between the plane of the C-C and C-H bonds and the axis of the p_Z orbital. The expression is not in widespread use because reliable estimates of the Q_{C-C-H}^H term are not available. For a freely rotating methyl group Equation 25 reduces to

$$a_{H} = \frac{1}{2} Q_{C-CH_{3}}^{H} \rho_{\pi}(C)$$
 (26)

There is no angular dependence and the $Q_{C-CH_3}^H$ term has been found to be a constant with a value of 58.6 gauss. For the general case of hyperfine interaction from a proton in a beta position an empirical equation

$$a_{H} = B_{1} + B_{2} \cos^{2} \theta$$
 (27)

is used which differs from Equation 25 in that it has a constant term B_2 ; a_H and θ have the same definitions as in Equation 25, and B_1 and B_2 are constants. From the theta dependence expressed in the above equation, it can be seen that β proton interactions will have a range of values depending on the radical geometry. The mechanism by which spin density is transferred to β hydrogens is not well understood. A hyperconjugative mechanism has been proposed which correctly predicts a positive spin density at the β hydrogen atom and gives the correct order of magnitude of the hyperfine interactions.

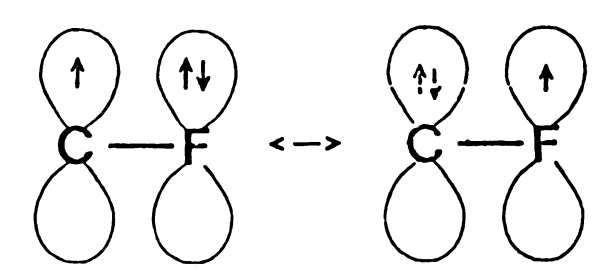
C. Nitrogen-and Amide-Proton Coupling

The hyperfine interactions of both $^{14}N(I=1)$ and amide protons are small and in many instances not well-resolved. Frequently, as an aid to the interpretation of spectra the amide protons are exchanged with deuterons which have a spin of 1 and a magnetic moment 0.3 that of hydrogen. In the solid state where linewidths are broad, the hyperfine splittings due to the deuterium atoms will not be seen and the spectrum will be simplified. The lines are also better resolved because the dipolar terms of deuterons are negligible.

D. α -Fluorine Coupling

The α -fluorine (I = 1/2) hyperfine tensor exhibits considerable anisotropy. In comparison with the α -proton analog, two features are apparent. First, although hydrogen (μ = 2.79) and fluorine (μ = 2.63) have similar magnetic moments, the hyperfine splitting values are quite different. Secondly, the largest element of fluorine tensor is directed perpendicular to the C-F bond and to the plane of the radical and has a positive sign, while that of the largest hydrogen tensor component is directed perpendicular to the C-H bond and in the radical plane, and has a negative sign. These facts suggest that spin polarization is not the dominant mechanism by which unpaired spin density is transferred to the fluorine atom. Fluorine has p orbitals

available to it which hydrogen lacks. Therefore, an α fluorine is capable of direct overlap with the odd electron orbital of a π radical. This would account for the relatively large anisotropies of the fluorine hyperfine splittings as well as the positive sign and direction of the largest component of the tensor. A spin polarization



mechanism whereby unpaired spin density is transferred through the C-F sigma bond is also possible. The effects of spin polarization are manifested as a slight but measurable deviation from axial symmetry.

There is no simple fluorine analog to McConnell's equation. An expression can be written for the fluorine isotropic splitting:

$$a_{\mathbf{F}} = Q_{\mathbf{C}-\mathbf{F}}^{\mathbf{F}} \rho_{\pi}(\mathbf{C}) + Q_{\mathbf{F}-\mathbf{C}}^{\mathbf{F}} \rho_{\pi}(\mathbf{F})$$
 (28)

However, the two terms, \mathbf{Q}_{C-F}^{F} and \mathbf{Q}_{F-C}^{F} , have not been quantitatively evaluated as yet.

E. α -Chlorine Coupling

Chlorine has two naturally occurring isotopes in measurable abundance. The 35 Cl (I = 3/2) isotope has a magnetic moment of 0.821 and an abundance of 75 percent while the 37 Cl (I = 3/2) isotope has a magnetic moment of 0.683. Since both isotopes have a nuclear spin greater than 1/2, each possesses a nuclear quadrupole moment. The hyperfine splittings are not completely resolved and components of the hyperfine patterns overlap. In addition the quadrupole interaction is as large as the hyperfine splitting for certain orientations of the magnetic field. If the magnetic field is not along the quadrupole symmetry axis (the C-Cl bond), there is competition between the electrostatic and magnetic interactions to align the nucleus and the resulting "forbidden" transitions become as intense as the "allowed" ones. For these reasons few chlorine-containing organic radicals have been successfully investigated in the solid state.

As is frequently observed in the case of fluorine tensors, the chlorine hyperfine tensor shows a slight deviation from axial symmetry due to the spin polarization effects. Again, there is no simple chlorine analog to the McConnell equation. An expression can be written for the chlorine isotropic splitting similar to that of fluorine and there is a means of evaluating the two terms, Q_{C-C1}^{C1} and Q_{C1-C}^{C1} .

Table III. Representative $\alpha\text{-fluorine}$ hyperfine interactions.

					
Radical	a iso (gauss)	B _{xx} (gauss)	B yy (gauss)	B _{zz} (gauss)	Ref.
$FC(CONH_2)_2$	63	137.0	-64	-73	5
FHCCONH ₂	56	133.0	-72	-60	59
F2CCONH2	75	103.0	-51	-51	60
-00CCFCF ₂ COO	71	79	-67	-12	61
CF ₃ CFCONH ₂	74	127	-66	-62	62
F2CCOONH4	72	116	-58	-58	63

Table I . Representative $\alpha\text{-chlorine}$ hyperfine interactions.

Radical	a iso (gauss)	B _{xx} (gauss)	B yy (gauss)	B _{zz} (gauss)	Ref.
CH ₂ Cl	2.8	17.72	2.47	4.05	13
снс1соон	3.7	16.3	-6.2	-10.1	11
CC1FCONH ₂	3.0	15.0	-0.2	- 2.8	12

$$a_{C1} = Q_{C-C1}^{C1} \rho_{\pi}(c) + Q_{C1-C}^{C1} \rho_{\pi}(c1)$$
 (29)

The σ - π parameters have been measured from the NMR chemical shifts of chlorine compounds. The values obtained are a_{C-C1}^{C1} = 4.7 gauss and Q_{C1-C}^{C1} = 29 gauss.64

VIII. EXPERIMENTAL

A. Preparation, Crystal Growth and Crystallography

Iodoacetamide was purchased from the Pierce Chemical Company, Rockford, Illinois, and was used without any further purification. Solutions of iodoacetamide in ethanol as well as in acetone were prepared. Similar crystals, in the form of thin plates, were grown within a day from either solution. Iodoacetamide had a tendency to form supersaturated solutions and several attempts were made before suitable crystals could be grown. The approximate dimensions were 0.1 mm x 3 mm x 5 mm. A crystal of iodoactamide and its axis system is shown in Figure 3.

Deuterated crystals were made by dissolving the material in D_2O , allowing enough time for the solution to equilibrate, and then extracting the solvent on a vacuum line. The procedure was repeated twice more. The deuterons exchange with the acidic protons to form $H_2ICCOND_2$.

A crystal of iodoacetamide with dimensions convenient for X-ray work was mounted on a goniometer head. Rather than align the crystal and assign a space group by the precession method as was done for bromomalonamide, it was decided to perform these operations directly with a diffractometer. A General Electric model XRD manual

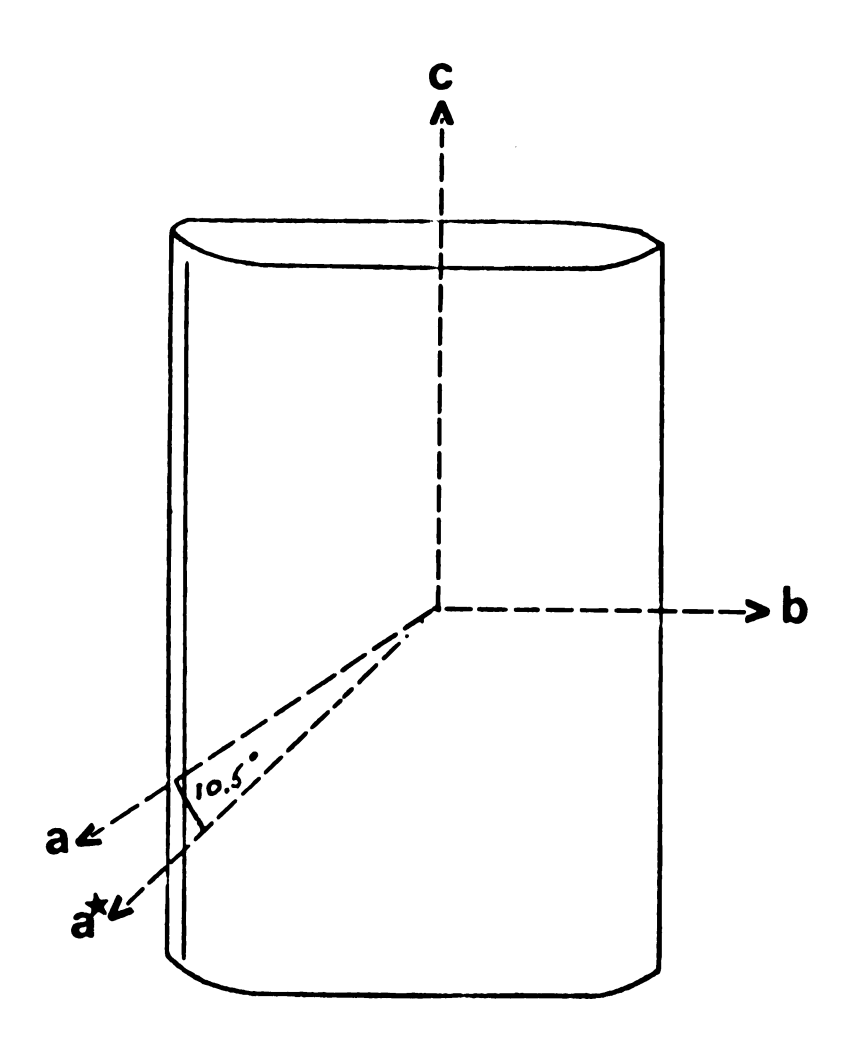


Figure 3. Axis system of iodoacetamide crystal.

diffractometer adapted for single crystals was employed with Cu K radiation ($\lambda = 1.5405 \text{ Å}$). Crystal structures had been previously reported for chloro- and bromoacetamide66 and it was found that these two structures were isomorphous. Although it did not necessarily follow that iodoacetamide would be isomorphous with these two, the assumption was not unreasonable; in addition, the space group to which these two belonged, $P2_1/c$, occurs quite commonly for organic compounds and can be uniquely determined from systematic absences (hol, & odd and Oko, k odd). In place of the photographs associated with the precession practice, reflections were graphed as a function of angle. When a sufficient number of reflections had been collected, the data were checked for various symmetry elements by positioning the diffractometer in an appropriate location. The presence or absence of a reflection will confirm or deny a possible symmetry element. In this manner, iodoacetamide was found to be monoclinic and assigned to space group, $P2_1/c$. The unit cell dimensions, a = 8.43 Å; b = 6.54 Å; c = 9.19 Å; and $\beta = 100.5^{\circ}$ precluded the possibility of iodoacetamide being isomorphous with chloro-and bromoacetamide.

The denisty, calculated on the basis of four molecules in the unit cell, is 2.43 gm cm⁻³. This compared favorably with the experimental density of 2.35 gm cm⁻³ from flotation in a mixture of iodomethane (ρ = 2.28 gm cm⁻³) and diiodomethane (ρ = 3.33 gm cm⁻³).

Iodoacetamide fluoresced in the X-ray beam and this created a large amount of background radiation. Therefore, the above results were rechecked and verified.

The symmetry elements for the $P2_1/c$ space group are a center of symmetry, a twofold screw axis about b and a mirror perpendicular to the b axis followed by a translation of 1/2 a unit cell length along the c axis. Since b is the unique monoclinic axis, the space group could equally well have been $P2_1/a$ merely by interchanging the a and c axes. A drawing of a typical crystal and the axis system chosen for EPR work are shown in Figure 3.

B. Sampling and Irradiation Procedures

Spectra were run of solutions, powders and single crystals, for both bromomalonamide and iodoacetamide. Each require separate and different preparations prior to irradi-

Reliable isotropic hyperfine splitting values were sought for α -bromine and α -iodine organic radicals. These values could be obtained from solution spectra although the radicals so formed need not necessarily be identical to those formed in powders and single crystals of bromomalon-amide and iodoacetamide. Solutions of di-tert-butylperoxide in several organic halogen compounds were prepared according to the procedure of Kochi and Krusic. These included diethylbromomalonate, dibromomethane, iodoacetamide, iodoacetic acid and sodium iodoacetate. The solutions consisted

of 75 percent di-tert-butylperoxide and 25 percent organic substrate by volume. No more than 20 ml of solution were required for an experiment. The solutions were placed in 4 mm OD quartz tubes and thoroughly degassed on a vacuum line. Ethane was added to depress the freezing point and the tubes were sealed while still under vacuum. In situ radiation of the solutions with ultraviolet light was used to generate free radicals. The light source was a Hanovia Model 977B-1 lamp equipped with a 1000 watt xenon-mercury arc bulb. An external water filter absorbed infrared radiation which could warm the sample. The light was focused with a concave quartz lens. Kochi and Krusic reported that the best signal-to-noise conditions were obtained at lowered temperatures, preferably below -700. A Varian variable temperature unit (model V-4540) maintained the desired temperature. Spectra were recorded in ten-degree increments of temperature beginning with -50° and going to -90° ; below -90°, the solutions froze. Irradiations invariably produced a single line attributable to the di-tert-butyl moiety, (CH₃)₃CCOO. This species scavenges from the organic substrate to produce the desired radical. Radicals formed in this manner are stable for several hours if the solutions are continuously exposed to the ultraviolet radiation.

Powders and single crystals were irradiated and examined at liquid nitrogen temperatures. If the samples were allowed to warm to room temperature, the ESR signal

would disappear within a matter of a few seconds. Gamma-rays from a ⁶⁰Co sample were the primary source of radiation but occasionally X-rays from a chromium target were used to produce free radicals. Irradiations ranged from three hours for bromomalonamide to five hours for iodoacetamide. The ⁶⁰Co γ-ray source delivered a dose rate of 2 x 10⁶ rad/hr or 2 x 10⁸ erg/g hr. Fine grinding is the only preparation of powders prior to radiation. This pulverizes any crystallites and eliminates the possibility of a spectrum with features of both a single crystal and a powder. Once the sample had been ground with a mortar and pestle, it was emptied into a 2-dram glass vial and capped. A gram or two of a powder sample sufficed for the purposes of the ESR spectroscopy experiment.

The vial was placed in a Dewar filled with liquid nitrogen. The γ -rays were able to penetrate the Dewar, liquid nitrogen, and glass vial to damage the samples. This was not the case with X-rays which have a limited penetrating ability so that samples must be kept as close as possible to the X-ray source. To accomplish this, the powder was sealed in a polyethylene bag with bits of Styrofoam to keep the bag afloat on top of the liquid nitrogen. The X-rays were then focused down onto the bag. In the case of either X-rays or γ -rays, an identical radical species was formed. The final step in the irradiation procedure was the same for both X- and γ -irradiated samples. At the completion of the irradiation process, the powder was quickly emptied

from its container into another Dewar filled with liquid nitrogen. This Dewar was specially constructed to fit into the ESR cavity. It was vacuum-jacketed, with silvered sides, and a Spectrasil quartz tip. Since powder samples have a tendency to bump due to the boiling action of the liquid nitrogen, a boiling chip and a quartz rod were inserted into the Dewar to minimize these effects. Signals were observed for as long as two weeks after the irradiation and it was assumed that the radical species formed by the irradiation had an indefinite life span if maintained at liquid nitrogen temperatures.

The procedure followed in obtaining spectra of a crystal was to first determine if it were truly single. Twin crystals were discarded since each portion of the crystal would have a different orientation in the magnetic field. The resulting spectra would be difficult to analyze and would also lead to an incorrect assignment of crystal symmetry. The axis systems for bromomalonamide and iodoacetamide were decided on the basis of external morphology and X-ray diffraction data.

There are no severe restrictions on crystal size as there are for X-ray diffraction work. The upper limit for the width and thickness is imposed by the diameter of the tip of the Dewar, 5 mm.

Two different approaches exist for the alignment and irradiation of crystals. In the first, which was eventually adopted for both bromomalonamide and iodoacetamide, the

crystal is mounted in the appropriate orientation on the flattened end of a copper wire which is attached to a long (~35 cm) glass tube. The crystal is held to the copper wire by a glue (Goodyear Pliobond) which does not lose its adhesive properties even at liquid nitrogen temperatures. The advantage to this procedure is that the crystal is mounted in a known preferred orientation prior to irradiation. The disadvantages are, first, that at least three different crystals are needed, one for each plane of rotation. Once glued in place, the crystal cannot be reclaimed. Secondly, the glue upon irradiation gives an ESR signal. These disadvantages were minimal in our case since several crystals are needed for other methods although in theory one will suffice. The signal from the glue is merely a nuisance since the A values of bromomalonamide and iodoacetamide are both very anisotropic. The glue signal appears as a single sharp line near the center of the spectrum due to the organic halogen radicals and was not confused with any of the transitions from either of the halogen radicals.

C. Spectrometer System

The experimental set-up consisted of a commercial Varian X-band spectrometer (V-4502-04) with a twelve-inch magnet and a multi-purpose cavity (V-4531). The field was modulated with a 100 kHz signal to facilitate detection and amplification of the ESR signal. The X-band system is designed to operate at a microwave frequency of 9.2 GHz

and magnetic field of 3000 gauss. The exact microwave frequency was measured with a T_S-148/UP U.S. Navy spectrum analyzer which covered an effective range of 9.0 to 9.5 GHz. An accurate determination of the magnetic field was made with a proton marginal oscillator connected to an electronic counter (Monsanto 151-A). The counter readout was in frequency units rather than magnetic induction units. A list of conversion factors is provided in the next section. The linearity of the magnetic field during a field sweep was maintained by a Hall probe.

The ESR signal could be displayed on an oscilloscope or printed out by an X-Y chart recorder (Hewlett-Packard 7005-B). Monitoring the oscilloscope display was a convenient way of optimizing the signal or locating a desired orientation quickly. The X axis of the chart recorder was a function of magnetic field position and a frequency marker from the proton marginal oscillator was placed on all spectra.

In ESR work, it is usual to record spectra in the first-derivative mode and this was done for powder samples. This was inconvenient for single crystals and the second-derivative signal, which closely resembles the true absorption signal and is easier to interpret and measure than the first-derivative signal, was used.

A variable temperature regulator (V4540) permitted the study of the temperature dependence of the spectra of free radicals.

D. Conversion Factors

Since several different units are in use at present by ESR spectroscopists, a partial list of conversion factors is provided here. The list is limited to the units usually encountered in the area of organic radicals. These units are MHz or, more commonly, gauss. However, computer programs require units of energy which are MHz or ergs.

$$g = \frac{0.714489 \times v_e(MHz)}{H(gauss)}$$

$$H(gauss) = 234.87465 \times v_p(MHz)$$

$$A(gauss) = \frac{A(MHz) \times 0.714489}{g}$$

$$A(gauss) = \frac{A(ergs) \times 1.0782 \times 10^{20}}{g}$$

A is the measured hyperfine splitting value, v_e is the klystron frequency, v_p is the proton marker frequency, H is the magnetic field magnitude.

VIII. RESULTS AND DISCUSSION

A. Bromomalonamide

1. Powder Spectra

The X-band ESR spectra of polycrystalline bromomalonamide and perdeuterobromomalonamide, each of which had been γ -irradiated and observed at 770K, are shown in Figures 4 (a) and 4(b), respectively. The powder spectrum of the deuterated amide shows hyperfine interaction with a single nucleus of spin I = 3/2, which must be bromine. The four "perpendicular" and four "parallel" bromine lines are visible in Figure 4, with the outermost peaks showing the expected fine structure due to the two bromine isotopes. Additional lines from interaction with a second nucleus of spin I = 1/2 are seen in Figure 4, and presumably arise from a proton; this doublet splitting of the parallel bromine lines is about 14 G. The ESR parameters obtained from the poweder spectra are listed in Table V. These results are consistent with the presence of the radical ·CHBrCONH2, •CDBrCOND2 in the deuterated compound, formed by loss or of an amide group on irradiation. It was similarly found⁵ in difluoromalonamide y-irradiated at 770K that an amide group was lost to give the radical 'CF2CONH2, while in



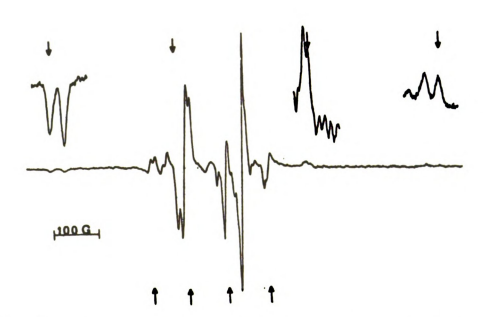


Figure 4. First derivative X-band ESR spectra of bromomalonamide powder γ -irradiated and observed at 77 0 K:

a) irradiated CHBr(CONH₂)₂, b) irradiated CDBr(COND₂)₂. The upper set of arrows indicates the parallel, and the lower set the perpendicular, line positions.

Table V. ESR parameters for the $\cdot \text{CHBr}(\text{CONH}_2)$ and $\cdot \text{CDBr}(\text{COND}_2)$ radicals.

Hyperfine Splittings and g values	Dire	ction Cos	ines ^a
Powder Da	ta		
$A_{ }(^{81}Br) = 290.0$			
A (⁷⁹ Br) = 267.6			
$A_{\perp} (81_{Br}) = 85.7$			
$A_{\perp} (^{79}Br) = 79.4$			
g = 1.9993			
$g_{\perp} = 2.0540$			
Single-Crystal	Data		
$A_{ }(^{81}Br) = 289.03 G^b$	0.585	0.811	0.008
A_{\perp} (81Br) = 83.79			
g = 1.9981 ^b	0.585	0.811	0.008
$g_{\perp} = 2.0428$			
$e^2Qq = 187 \text{ MHz}$	0.585	0.811	0.008

aDirection cosines with respect to the crystallographic a, b, c, axes.

bCorrected for second-order effects and so different from powder values.

 $\gamma\text{-irradiated}$ CF_3CONH_2 the carbon-carbon bond was also broken and both the $\dot{\text{CONH}}_2$ and $\dot{\text{CF}}_3$ fragments identified from ESR spectra. 60

2. Single-Crystal Spectra

All single-crystal data reported are for the deuterated radical which was employed to simplify the spectra since the maximum deuterium splitting is less than the linewidths ($\simeq 10 \, \mathrm{G}$) and only the bromine splittings are resolved. Also, the bromine lines become narrower because unresolved splittings from the amide hydrogens are reduced on deuteration. Parameters listed are for the $^{81}\mathrm{Br}$ isotope; the ratio of the hyperfine splittings $A(^{81}\mathrm{Br})/A(^{79}\mathrm{Br})$, when measured, was always close to the ratio of the magnetic moments of the isotopes (1.08).

The X-band spectrum of γ -irradiated CDBr(COND₂)₂ at 77°K is shown with the magnetic field parallel to the a, b and c crystal axes in Figures 5, 6, and 7. The lines are plotted versus the angle of rotation about the a, b, and c axes of the crystal in Figures 8, 9, and 10 respectively. In general, there are two magnetically nonequivalent sites except when the field lies along an axis; however, with the magnetic field in the ab plane no site splitting is observed. The irregular line spacings and intensities, and the appearance of forbidden ($\Delta m_{\rm I} = \pm 1, \pm 2$) transitions, indicate that the nuclear quadrupole interaction term cannot be neglected.

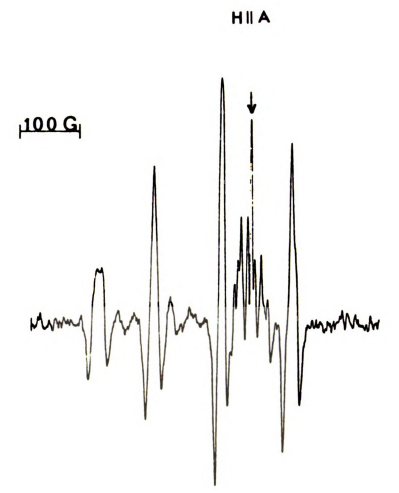


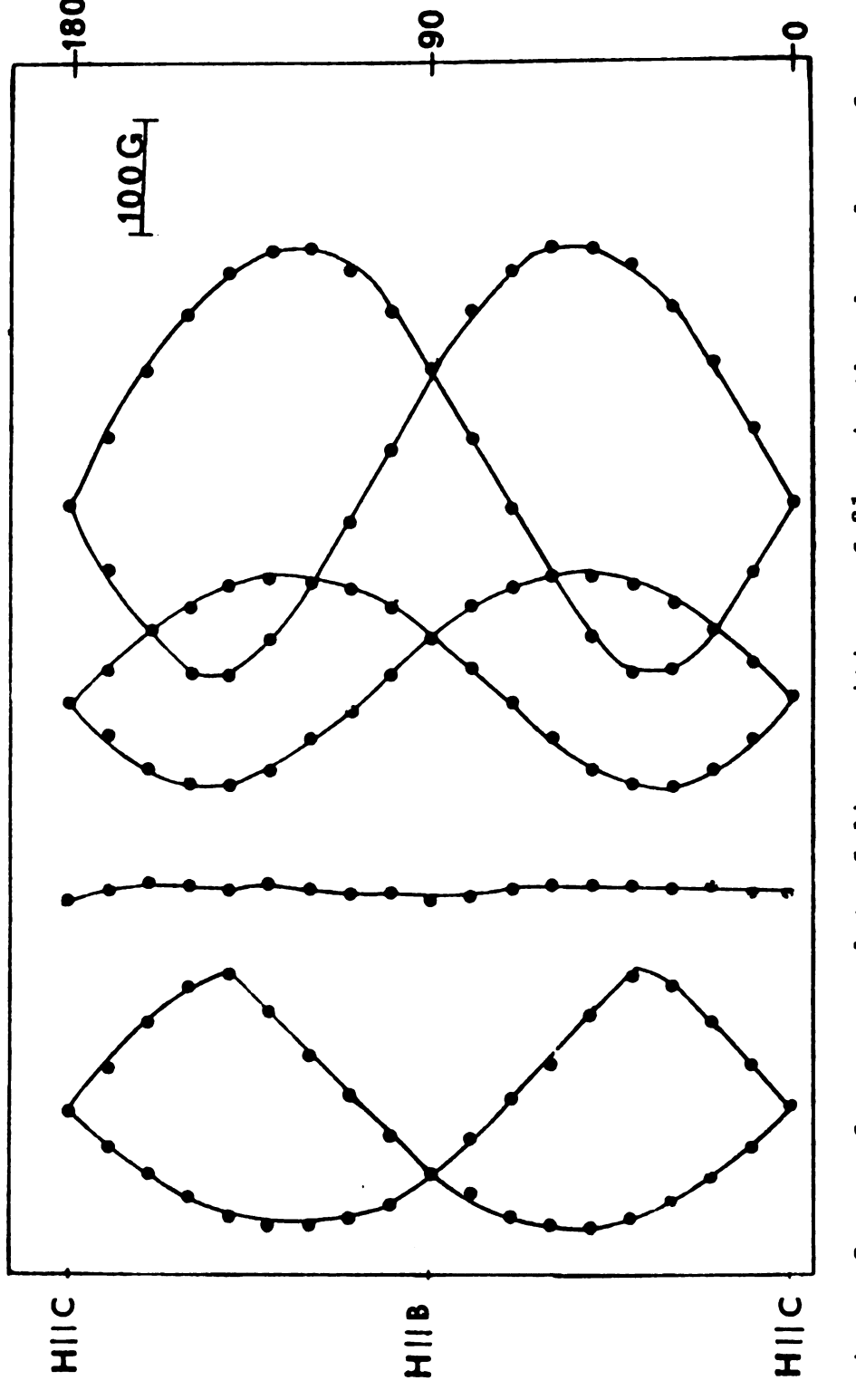
Figure 5. Second-derivative single-crystal ESR spectrum of CDBrCOND₂ with the magnetic field along the a crystallographic axis. Arrow indicates the •COND₂ radical.



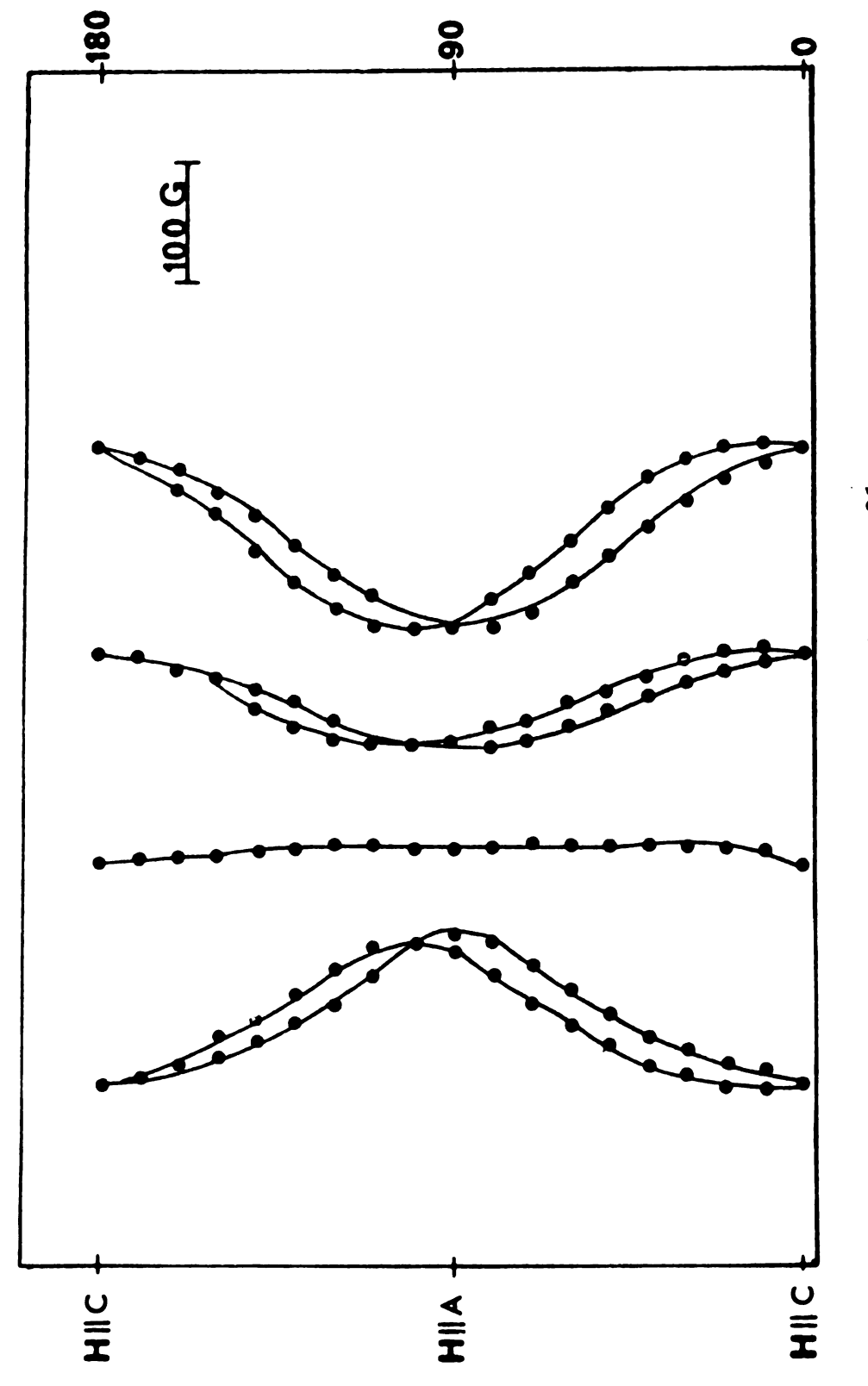
Figure 6. Second-derivative single-crystal ESR spectrum of CDBrCOND2 with the magnetic field along the b crystallographic axis.



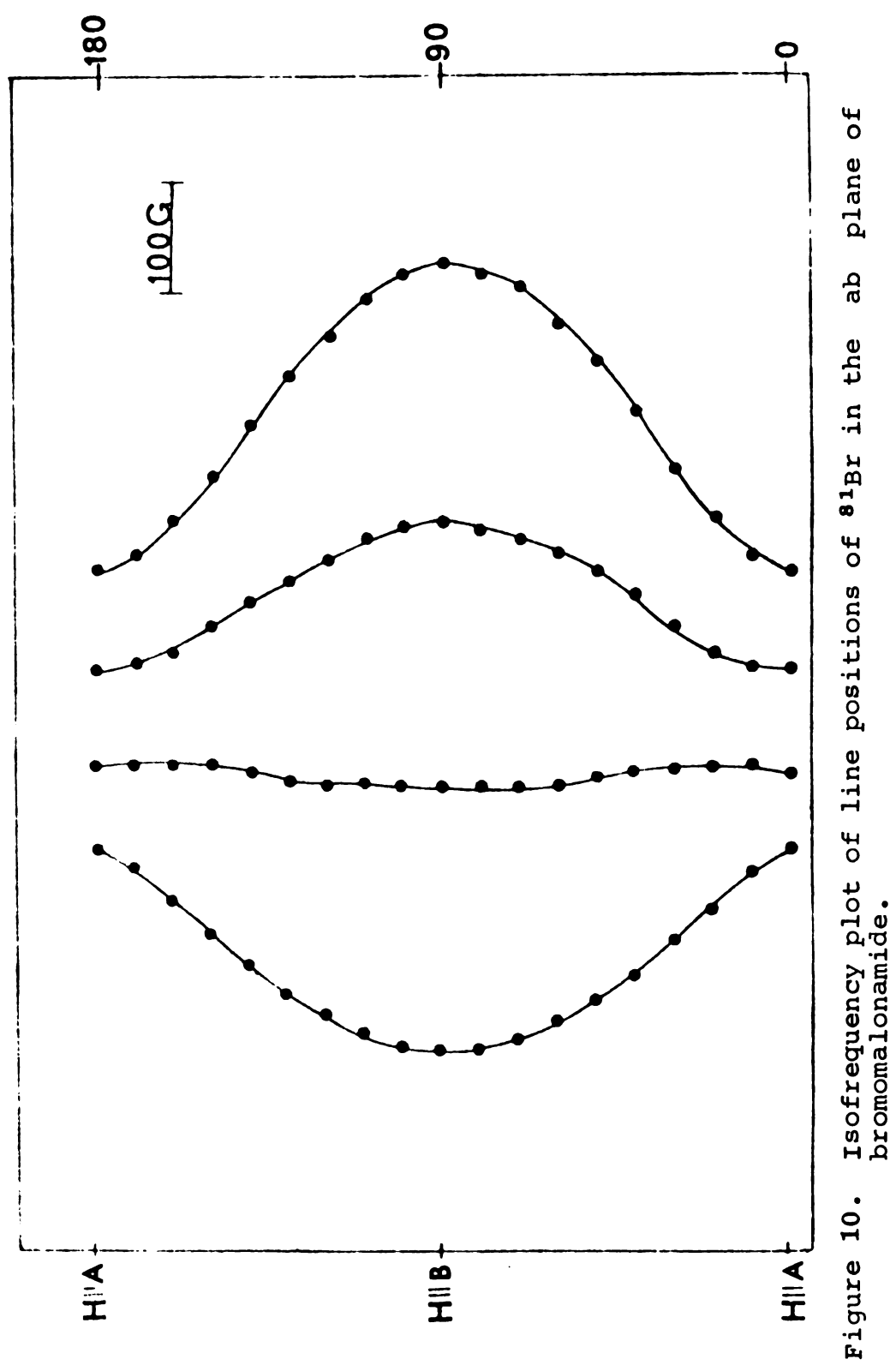
Figure 7. Second-derivative ESR single-crystal spectrum of CDBrCOND₂. The stick diagrams show the line positions and intensities calculated with the complete Hamiltonian for a) $q_{zz} \perp A_{||}(Br)$.



Isofrequency plot of line positions of $^{81}\mathrm{Br}$ in the bc plane of bromomalonamide. Figure 8.



plane of ac Isofrequency plot of line positions of ⁸¹Br in the bromomalonamide. Figure 9.



The spectra were analyzed using the spin Hamiltonian

$$\mathcal{K} = \bar{\beta}\hat{H} \cdot \bar{g}^{>}S^{>} + \bar{S} \cdot A^{\bar{B}^{+}} \cdot I^{\bar{B}^{+}} + I^{\bar{B}^{+}} \cdot \bar{Q}^{+} \cdot I^{\bar{B}^{+}} + g_{N}\beta_{N}H \cdot I^{\bar{B}^{+}}$$

and the computer program MAGNSPEC, 67 which provides the positions and intensities of the lines for any choice of input parameters. A preliminary value of the quadrupole interaction constant $Q' = 3e^2Qq/4I(2I + 1)$ was obtained from the line positions in the parallel and perpendicular orientations of the A tensor by use of the second-order perturbation theory expressions

$$hv = \beta g_{\parallel} H_{\parallel} + A_{\parallel} m_{I} + (A_{\perp}^{2}/2hv) \{I(I+1) - m_{I}^{2}\}$$
(30)

$$hv = \beta g_{\perp} H_{\perp} + A_{\perp} m_{I} + (A_{\parallel}^{2} + A_{\perp}^{2})/4hv \{I(I+1) - m_{I}^{2}\}$$

$$- \frac{Q'm_{I}}{2A} \{2I(I+1) - 2m_{I}^{2} - 1\}$$
(31)

Here $g_{\parallel \parallel}$, g_{\perp} , $A_{\parallel \parallel}$, A_{\perp} are the principal components of the g and hyperfine interaction tensors, respectively. In all the calculations it was assumed that the g and A(Br) tensors have axial symmetry and that their principal axes are coincident. Equations 30 and 31 also assume that q_{zz} , the maximum quadrupole interaction, is parallel to $A_{\parallel \parallel}(Br)$. Agreement between calculated and observed spectra indicates that these assumptions are justified.

The principal values of the g and $A(^{81}Br)$ tensors, along with their direction cosines relative to the crystal axes, are shown in Table V.

A more precise value of Q' was obtained by calculating spectra with the computer program MAGNSPEC⁶⁷ for comparison with the experimental spectra at selected orientations of the magnetic field. Since q_{zz} might also be perpendicular to $A_{||}(Br)$, spectra were also calculated on that assumption. The "forbidden" transitions in the observed spectra were best accounted for with $q_{zz}||A_{||}(Br)$. A value $e^2Qq(^{81}Br)$ = 187 MHz was obtained in this way (Table V).

The relative signs of the principal components of the bromine hyperfine splitting tensor were not determined in this work since the $\Delta m_{\tau} = \pm 1$, ± 2 lines could only be followed for limited ranges. The largest principal value may, however, be assumed to be positive since this found to be true for the halogen tensors in all α -halo radicals studied; it has been attributed to the direct transfer of positive spin from the carbon $2p_{\pi}$ orbital into the α -halogen np_{π} orbital. Since the tensors show axial symmetry, there are then two possible sign choices for $(A_{\mid \mid}, A_{\mid})$, (++) or (+-). A knowledge of a iso (Br) would help in selecting the proper set but all attempts to obtain an isotropic spectrum of an α -bromo radical have failed so far. Various bromocarbon derivatives were irradiated in an adamantane matrix and several organic bromides and dibromides were photolyzed in the presence of di-tert-butylperoxide but none of these experiments led to an ESR spectrum attributable to a brominecontaining radical.

3. Structure of the Radical

Since it was not possible to determine the relative signs of $A_{\parallel \parallel}$, A_{\perp} the consequences of each of the two possible choices will be examined. The isotropic and anisotropic bromine hyperfine interaction terms are shown in Table VI for each choice assuming that the observed tensor is of the form (a + 2B, a-B, a-B). Comparable values for related halogen-substituted radical are also given; in the case of the chloro- and fluoro-radicals, the relative signs are known. Unpaired spin densities in the bromine 4s and 4p orbitals were estimated for each choice using the values 68 $a_0(Br) = 8370$ G and $2B_0(Br) = 495$ G from Hartree-Fock calculations.

Since the spectrum shows hyperfine interaction from one bromine and one hydrogen nucleus, and since the spectrum of a \cdot CONH₂ fragment is observed, the most probable structure for the radical is \cdot CBrHCONH₂. The ESR data for \cdot CHFCONH₂ and \cdot CHClCONH₂^{59,11} lead to the conclusion that they are π -electron radicals with the trivalent carbon and the three atoms bonded to it nearly in a plane. Substitution of a less electronegative substituent, bromine, should favor a more planar arrangement⁶⁹ hence \cdot CBrHCONH₂ might be expected to also be a planar π -electron radical.

If this is correct then the choice of positive signs for both $A_{[\]}$, $A_{[\]}$ (Br) would be favored since the π spin density, $\rho_{\pi}(Br)$ = 0.275, is then not unreasonable. While

Components of the halogen hyperfine splitting tensors and spin densities in haloacetamide radicals. Table VI.

Radical	Relative Signs Ā	a _{iso} (x) gauss	B gauss	ρ _{ns} (x)	$\rho_{\mathbf{np}_{\pi}}(\mathbf{x})$	$ ho_{2_{\mathbf{P}_{\pi}}}(\mathtt{c})$	Ref
·CHFCONH2	(+)	+56.4	(132.7,-60,-72)	0.0030	0.0030 0.119(X=F)	0.80	59
· CHC1CONH2	(+)	+ 3.7	(16.3, -6.2, -10.0)	0.0022	0.0022 0.15(x=c1)	0.78	59
· CHB r CONH2	(+ + +)	+152.2	(136.8, -68.4, -68.4)	0.018	0.275(X=Br)		This work
	(+)	+ 40.5	(249, -124, -124)	0.0045	0.50		
·CHICONH2	(+ + +)	+145.0	(96, -48, -48)	0.0198	0.212(X=I)		This work
	(· · · +)	+ 16	(225, -112, -112)	0.0022	0.495		

The observed tensors, $\overline{\overline{A}}(X)$, have been decomposed into isotropic, (a_{1SO}) , and anisotropic, $\overline{\overline{B}}(X)$, components assuming the relative signs of column 2 and assuming that $A_{max}(X)$ is positive. In the case of the chloro-and fluoro-radicals the relative signs shown were found experimentally. considerably larger than $\rho_{\pi}(\mathbf{F})$ and $\rho_{\pi}(\mathbf{Cl})$ in the chloro-and bromo-radicals, the latter are increasing with size of halogen. The choice of opposite signs for $\mathbf{A}_{\parallel \parallel}$, $\mathbf{A}_{\perp}(\mathbf{Br})$ leads to the very high value $\rho_{\pi}(\mathbf{Br}) = 0.50$ which would be appropriate for a σ^* radical. Thus, $\rho_{\pi}(\mathbf{Br}) = 0.526$ in $\cdot \mathbf{FBr^{70}}$ and is 0.40 in $(\mathbf{CH_3})_2\mathbf{S^{-Br}},^{22}$ both of which are said to be σ^* radicals. It should be noted that in these bromine is bonded to an atom carrying a lone pair of electrons so delocalization of the odd electron is facilitated.

As discussed in more detail below, the isotropic splitting on either sign choice is much larger than would have been anticipated on the basis of the sketchy knowledge of a(Br) values available in the literature. However, even the value $a_{iso}(^{81}Br) = 152.2$ G associated with the preferred choice of all positive signs for $A_{||}$, $A_{||}$ corresponds to only a small spin density in the bromine s orbitals, $\rho_s(Br) = 0.018$. This may not be unreasonable since ρ_{S} -might be expected to increase with $-\rho_{\pi}$ -if it arises, in part at least, from spin polarization of the bromine s by the bromine p odd-electron density. The large value $\rho_{\rm s}$ might also be associated with some deviations from planarity since it has been shown that in a series of fluorine-substituted radicals $a_{iso}(F)$ increases with θ , the angle of bending from planarity.8 In any case both $\rho_{\text{S}}(\text{Br}\,)$ and $\rho_{\pi}(\text{Br}\,)$ are close to the analogous values in •CHICONH $_2$, which appears to be a π -electron radical.

One might expect that $\rho_{n\pi}(x)$, and with it $\rho_{ns}(x)$, would vary in the series 'CHXCONH₂ (X = F, Cl, Br, I) as the overlap integral $S(2p_{\pi},np_{\pi})$, since odd-electron density is believed to be largely transferred to the halogen by direct overlap. Values of ⁷¹ $S(2p_{\pi},np_{\pi})=0.122$, 0.147, 0.115 are estimated for n = 2, 3, 4, 5 so this integral appears to show a maximum at bromine just as $\rho_{n\pi}(x)$ and $\rho_{ns}(x)$ do.

The axial symmetry observed for the bromine hyperfine splitting tensor is surprising since the fluorine tensors in ·CFXY type radicals show deviations from axial symmetry of 4-10 G, generally attributed to spin polarization of the $_{\rm C}$ bonding electrons of the C-F bond; $^{8-10}$ similarly, the chlorine tensors in ·CClXY type radicals $^{11-15}$ show deviations of 2-4 G. These values correspond to $_{\rm C}(\rm np_{_{\rm C}}) \simeq 0.01$ and one might expect similar polarizations of the $_{\rm C}$ bonding electrons in bromo radicals. However, the present bromine tensor is axially symmetric within experimental error, as was the bromine tensor reported for $_{\rm CH_3})_2 \rm SBr;^{22}$ also, it is found that the iodine tensor in ·CHICONH2 is nearly axially symmetric. 72

The value of g_{\perp} is quite large, while g_{\parallel} is somewhat below the free-spin value, as would be expected for a radical in which the odd electron is partly on bromine and g_{\perp} is in the radical plane. Thus, the g values for the radical •CHICONH₂ behave in the same way as the g values reported here. It is interesting that g_{\parallel} = 1.999,

 $g_{\perp} = 2.070(2.075)$ for $(CH_3)_2SBr$, which has been described as a σ^* radical by analogy with Br_2^- , and so would have g_{\parallel} perpendicular to the S-Br bond.

The nuclear quadrupole interaction $e^2qQ = 187 \text{ MHz}$ is rather smaller than typical values ($\sim 400 \text{ MHz}$) for diamagnetic bromocarbon derivatives obtained by NQR spectroscopy. 73 In addition, q_{zz} lies along the C-Br bond in the latter compounds. However, with an odd electron spin density of $\simeq 0.27$ in the bromine p_{π} orbital it is perhaps not surprising that q_{zz} is normal to the radical plane in the present case. In $(CH_3)_2SBr$ it is also found that q_{zz} and $A_{||}(Br)$ are parallel 22 but, if that radical is a σ^* radical as proposed, $A_{||}(Br)$ would be parallel to the S-Br bond. No theoretical studies of quadrupole coupling in free radicals appear to have been made.

4. Other Considerations

Other possibilities for the structure of the radical cannot be eliminated at this time since the only other single-crystal studies of radicals showing bromine hyperfine interactions which are available at present are for species of rather different types. The V-centers, such as $\cdot Br_2$ and $\cdot FBr$, are σ^* radicals 70 and the data for $(CH_3)_2S$ Br were also interpreted on that basis. Our values of $A_{||}(Br)$, $A_{||}(Br)$, $A_{||}(Br)$, and $G_{||}(Br)$ are rather similar to those reported for $(CH_3)_2SBr^{22}$ so there is a possibility that our paramagnetic species is similar. Such a radical might be obtained

by loss or gain of an electron from the molecule as a whole $[CHBr(CONH_2)_2]^+$ or -. No species of this type, showing halogen hyperfine interactions, appears to have been thoroughly established among carbon-centered radicals. Also it would appear to be difficult to delocalize 50% or more of the odd-electron density from bromine onto carbon, or the rest of the molecule, when carbon is bonded to four atoms and so has no vacant orbital or lone pair. Further, one component of the bromine tensor should then lie along the C-Br direction in the undamaged crystal. This is not the case since $A_{[]}(Br)$, which should lie along the C-Br bond direction in a σ^* radical, makes an angle of 78^0 with the C-Br direction in the undamaged bromomalonamide crystal.74

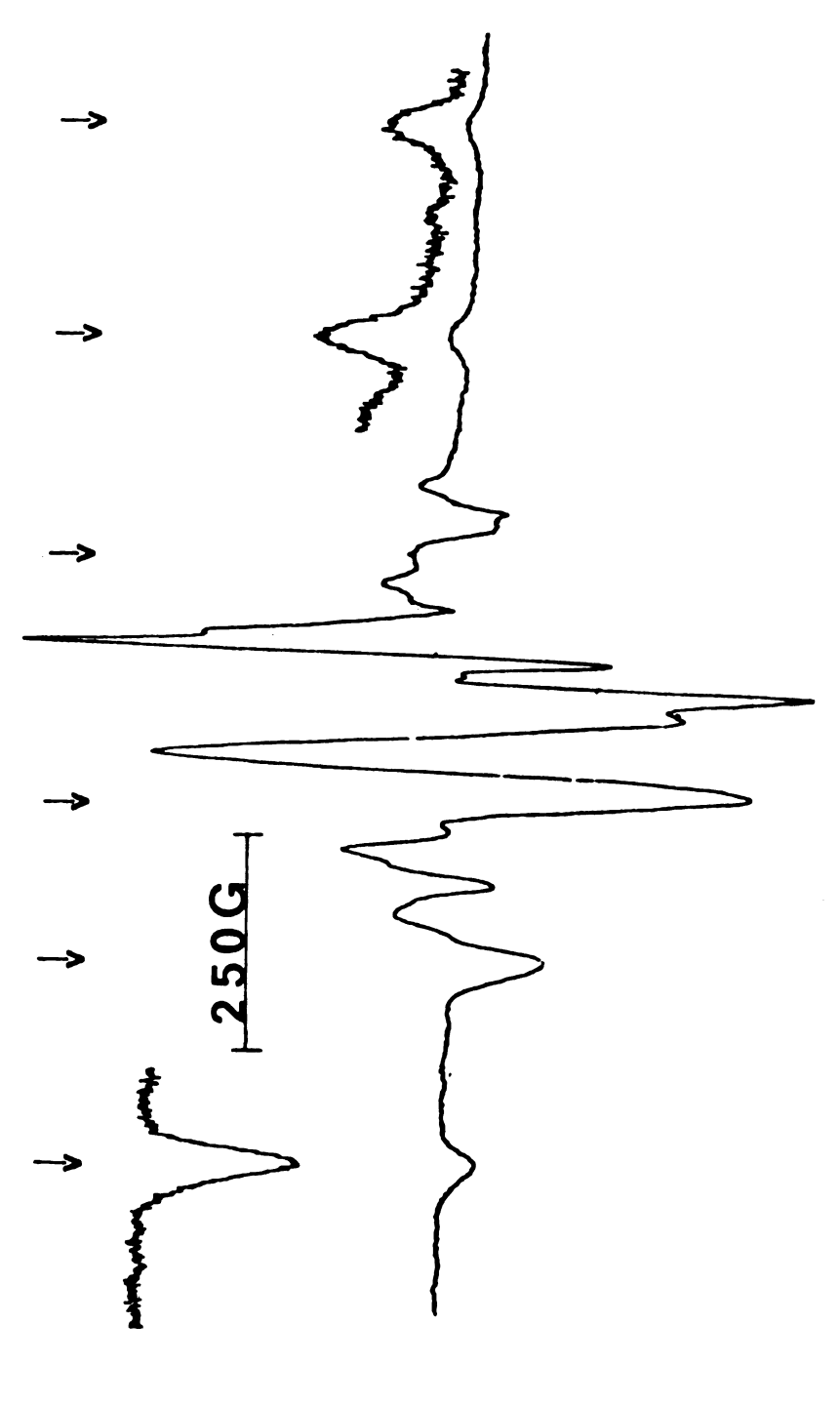
It is also disturbing that the values of the principal components of the g and bromine hyperfine splitting tensors which we find differ so extensively from the values (based on powder data) reported by Mishra, et al.²⁶ for some radicals believed by them to be of the type ·CBrRR'. Thus, they find a_{iso}(⁸¹Br) = -5.3 G, anisotropic ⁸¹Br tensor components (107, -48, -75) and g tensor components (2.002, 2.016, 2.038) for a radical which they identify as ·CHBrCOOH, while we find a_{iso}(⁸¹Br) = 152.2, anisotropic ⁸¹Br tensor components (136.8, -68.4, -68.4) and g tensor components (1.9981, 1.9981, 2.0428) for ·CHBrCONH₂. Since those radicals should have essentially identical ESR parameters, the radicals must be of rather different types.

At present the radical studied in this investigation is considered to be the π -electron radical ·CHBrCONH₂ since the radical in irradiated iodoacetamide appears to be ·CHICONH₂ and the latter is also characterized by a large, presumably positive, halogen hyperfine splitting, near axial symmetry of the A(X) tensor and g_{\parallel} below the free-spin value. Further work with related species, and the direct observation of isotropic bromine and iodine hyperfine interactions, will be needed to establish the structures of these species.

B. Iodoacetamide

Powder Spectra

The ESR spectrum of iodoacetamide powder irradiated and observed at $77^0\mathrm{K}$ is shown in Figure 11. A set of six peaks separated by an average spacing of 242 G are indicated by the vertical arrows. These may be identified as the parallel components of the $A(^{127}\mathrm{I})$ tensor $(^{127}\mathrm{I}, \mu = 2.7939, \mathrm{I} = 5/2, Q = -0.75, 100\%$ natural abundance) since the splitting is too large to arise from any other magnetic nucleus. As a result of the large iodine hyperfine interactions and the iodine quadrupole moment, the spectra would not be expected to be described by first-order perturbation theory and the irregular spacings of the six lines are therefore ascribed to second-order effects. The lines are quite broad (about 40 G) and no splittings from interaction with



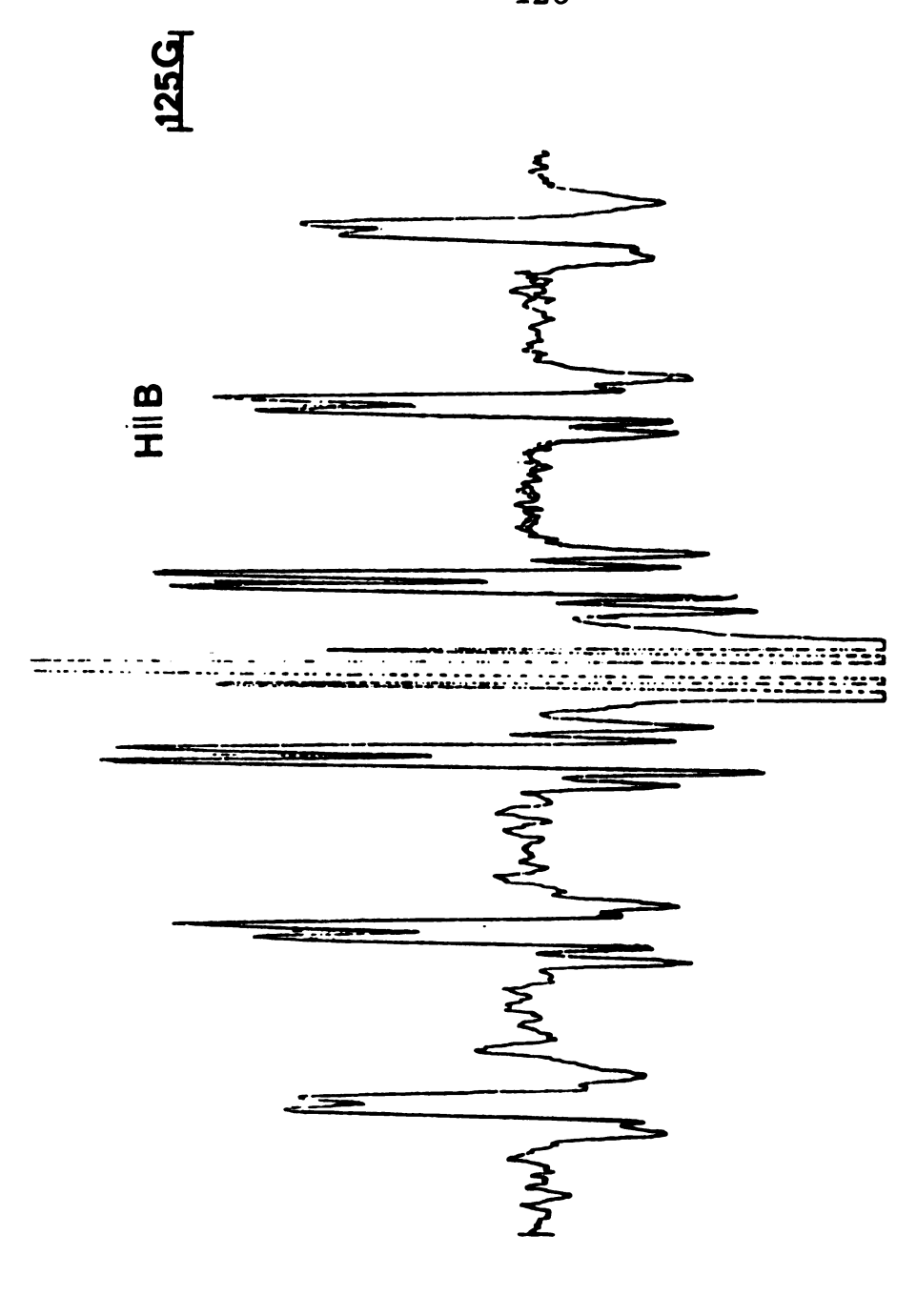
The arrows indicate X-band powder spectrum of irradiated iodoacetamide. the $^{12}7\mbox{I}$ parallel hyperfine line positions. Figure 11.

any other nuclei could be resolved. A spectrum of γ -irradiated CH₂ICOND₂ powder showed no appreciable line sharpening indicating that it is unresolved nitrogen and α -proton, rather than amide hydrogens, hyperfine splitting which contribute more to the line broadening. The powder spectra also provided the approximate values $g_{\parallel} \simeq 1.9900$ and $A_{\perp}(^{127}I) \simeq 100G$ which aided in the analysis of the single crystal spectra.

2. Single Crystal Spectra

With the magnetic field along a crystallographic axis, or in the a*c plane, a set of six doublets is obtained (Figure 12, H | | b); these twelve lines have nearly equal intensities. The large sextet splitting must result from interaction with one iodine nucleus, as shown also by the powder spectrum, while the small doublet splitting is the order of magnitude expected for interaction with a single proton. When the magnetic field is in an arbitrary direction a second set of six doublets with different spacings is observed indicating that there are, in general, two magnetically inequivalent sites. Often the second set consists only of six broad lines, the proton hyperfine splitting having been lost in the line width, and it was, therefore, difficult to obtain an accurate $A(^1H)$ tensor.

The radical was assigned the structure •CHICONH₂ based on these results. This radical is anticipated on the basis of the earlier analysis of irradiated fluoro- and chloroacetamide which form •CHFCONH₂ and •CHClCONH₂, respectively.

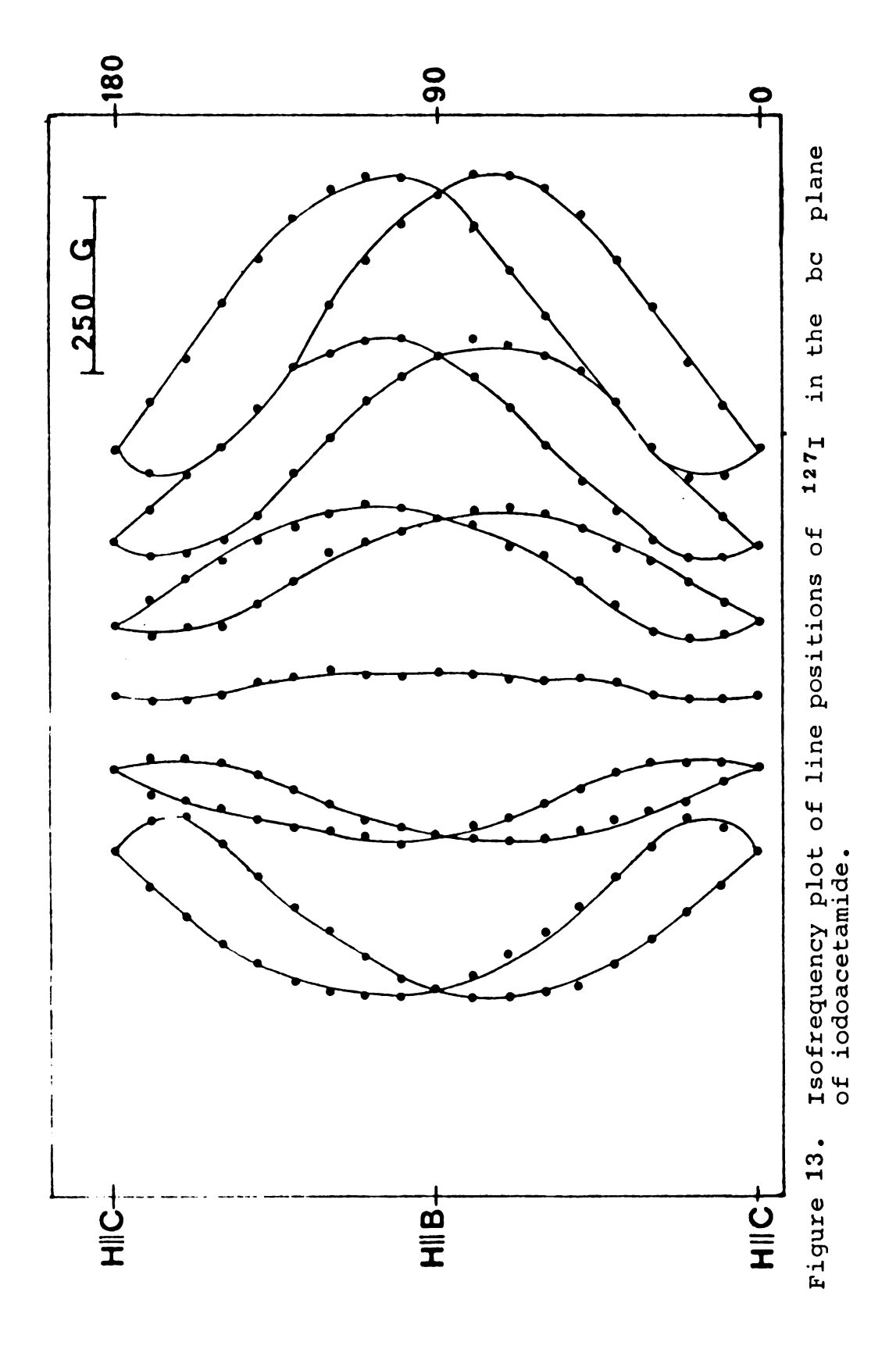


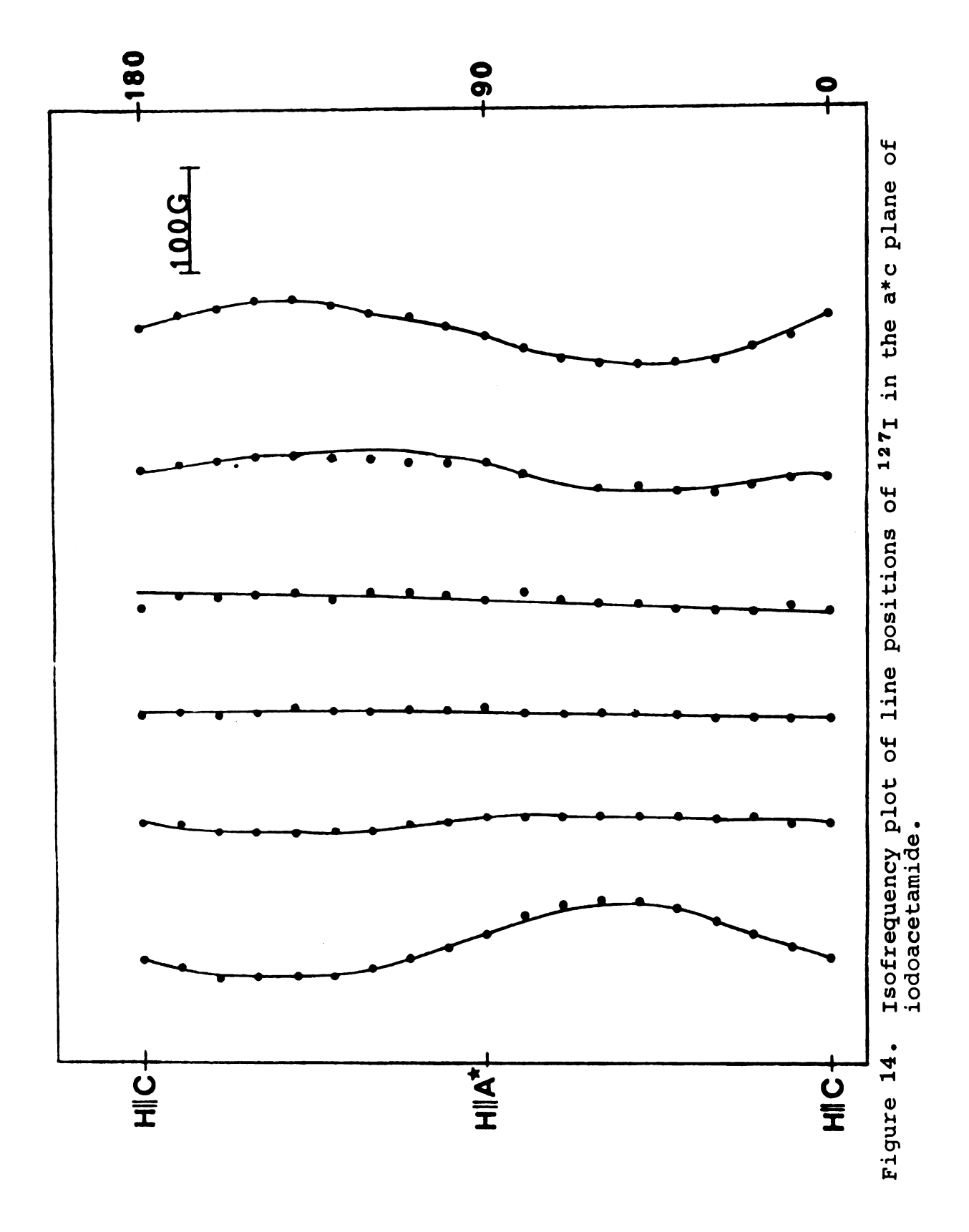
X-band second-derivative ESR spectrum of a single-crystal of irradiated iodoacetamide. The magnetic field is along the b axis. Figure 12.

3. g and $A(^{127}I)$ Tensors

The appropriate spin Hamiltonian for analysis of these spectra is

where the symbols have their usual significance and
$$Q' = 3e^2q_{zz}Q/4I(2I-1)$$
. The magnetic field positions for the components of the iodine multiplets are shown as a function of magnetic field orientation in bc, a*c, and a*b planes in Figures 13, 14, and 15, respectively. The iodine hyperfine interaction tensor and the g tensor were obtained from these data by the method of Waller and Rogers. The unequal spacings of the lines show that second-order effects are important. These were minimized by using, at each orientation, one-fifth of the separation between the outer lines. In this way the g and $A(^{127}I)$ tensors may be obtained with minimum error from neglect of the quadrupole interaction term. The principal components and direction cosines obtained in this way for the $A(^{127}I)$ and g tensors are shown in Table VII; the relative signs of the principal components of $A(^{127}I)$ were not determined in this work, both the $A(^{127}I)$ and g were found to be axially symmetrical within experimental error and share a common axis system.





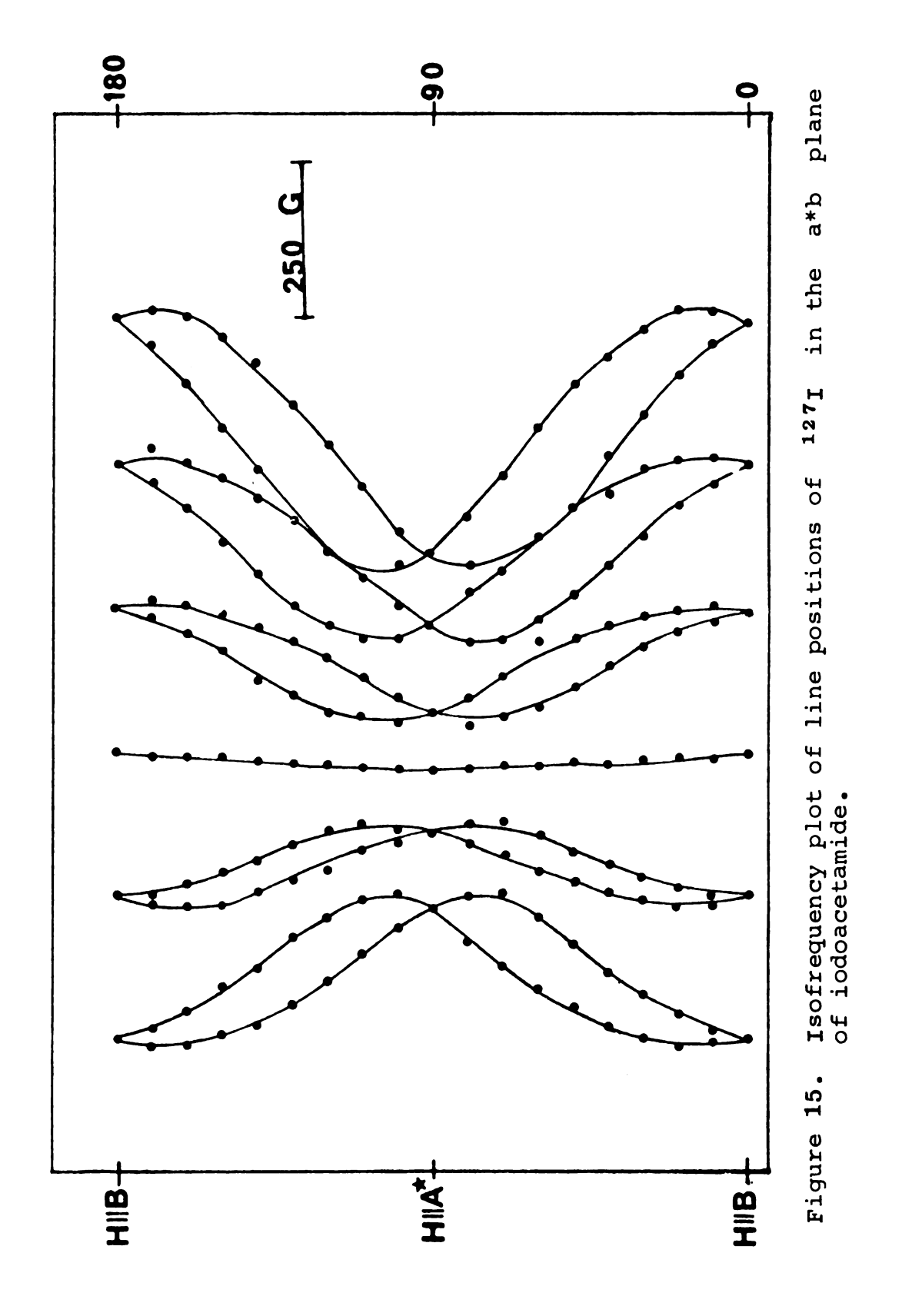


Table VII. ESR parameters for the radical •CHICONH2.

					
Principal Tensor Components a	Direction Cosines ^b				
Iodine Hyperfin	e Interac	tion			
$A_{[]}(^{127}I) = (+) 242.0 G$	0.269	0.935	0.230		
$A_{\perp}^{(127I)} = 95.75$	-	-	-		
g Ten	sor				
g = 1.9902	-0.271	0.930	0.236		
g = 2.0423	-	-	-		
Hydrogen Hyperfi	ne Intera	ction ^C			
$A_{XX}(H) = (-) 27.5 G$	0.746	0.192	0.637		
$A_{yy}(H) = (-) 8.7$	-0.227	0.974	-0.028		
$A_{ZZ}(H) = (-) 19.0$	-0.626	-0.123	0.770		
Iodine Nuclear Quadrupole Interaction d					
$e^2qQ = 216 \text{ MHz}$	0.269	0.935	0.230		

^aSigns in parentheses are assumed on the basis of known signs in similar radicals.

bwith respect to a*, b, c axes of the crystal.

^CThe probable error in principal components, and particularly in direction cosines, is rather large for this tensor because the proton splitting was not always resolved.

The direction cosines for the maximum quadrupole interaction appear to be the same as for A but the spectra are not very sensitive to changes in them.

4. A(H) Tensor

Although the proton hyperfine splittings could not be resolved in all orientations, reasonably good values of the principal components of the A(H) tensor and their direction cosines were obtained by the method of Waller and Rogers; 75 these are given in Table VII.

5. Quadrupole Interaction

A preliminary value of Q' (Equation 32) was obtained by the method of Bleaney. The value listed in Table VII was then modified by fitting the experimental line spacings to those calculated by the computer program MAGNSPEC with various input parameters. The spacings are not very sensitive to Q' so the probable error is rather large.

6. Structure of the Radical

The iodine hyperfine interaction tensors may be broken down into an isotropic component, (a_{iso}) , and a dipolar tensor (2B, -B, -B) in two ways depending on choice of relative signs for the components of $A(^{127}I)$. In all halogen tensors for π -electron radicals for which the relative signs of the principal components have been measured, the maximum value is normal to the radical plane (here taken as the z axis, with the x axis directed along the C-I bond), and is positive. If it is assumed that $A_{||}(^{127}I)$ is positive there exist two sign choices (+ + +) and

(+ - -) and values of a_{iso} and 2B derived for each choice are listed in Table VIII. Estimates of $\rho_{5s}(I)$ and $\rho_{5p_{\pi}}(I)$ corresponding to each choice were obtained by use of the Hartree-Fock values⁶⁸ for $a_0(I_{5s})$ and $2B_0(I_{5p})$. The choice of opposite signs (+ - -) leads to an odd-electron spin density of 0.50 in the iodine $5p_{\pi}$ orbital which is unreasonably large if the radical is the π -electron species, ·CHICONH₂. The choice of all positive signs (+ + +) leads to a value of $\rho_{5p_{\pi}}(I) = 0.21$ which is comparable with the values $\rho_{3p_{\pi}}(C1) = 0.15^{11}$ and $\rho_{4p_{\pi}}(Br) = 0.27^{76}$ for the ·CHClCONH₂ and ·CHBrCONH₂ radicals; furthermore, the value of $\rho_{5s}(I) \simeq 0.02$ is close to the value $\rho_{4s}(Br) = 0.018$ found for ·CHBrCONH₂.

Table VIII. Components of the iodine hyperfine splitting tensor and spin densities in the iodine valence orbitals.

Radical	Relative Signs \(\overline{A}\)	a _{iso} (I) G	2 _B (1)	ρ _{5s} (I)	ρ ₅ ρ _π (Ι)
·CHICONH ₂	(+ + +) (+)	145.0 16.0	96 225	0.0198 0.0022	0.21

The near axial symmetry for the A(127I) tensor indicates negligible polarization of the iodine $5p\sigma$ orbitals by the odd electron spin. This is puzzling since the estimated spin densities $\rho_{2p_{\sigma}}(F)^{59}$ and $\rho_{3p_{\sigma}}(Cl)^{11}$ in

•CHFCONH₂ and •CHClCOOH are -0.016 and -0.026 respectively. However, it is consistent with the observation that the bromine tensor is axially symmetrical in radicals
•CHBrCONH₂⁷⁶ and (CH₃)₂SBr.²² The anisotropy of the g tensor found here is large and increases in the series
•CHXCONH₂ as the magnitude of the spin-orbit coupling parameter increases, as would be expected. Values of g below free spin may be associated with low-lying empty d orbitals in bromine and iodine.

The proton hyperfine splitting tensor is about 10-20% smaller than that found for simple, planar π electron radicals. The spin-density in the carbon $2p_{\pi}$ orbital would then be estimated as 0.75-0.90 from McConnell's rule. This estimate agrees quite well with the ~ 0.77 predicted by difference using the spin densities of Table VIII. This agreement is strong support for the structure 'CHICONH2 for the radical.

The quadrupole interaction $e^2qQ=216$ MHz is considerably smaller than typical values 73 for aliphatic iodocarbon derivatives obtained from NQR work ($e^2qQ\simeq 1600-1900$ MHz) and the direction appears to be normal to the radical plane whereas it is along the C-I bond in diamagnetic molecules. These differences may be the result of the presence of large unpaired electron population in the iodine p_{π} orbital.

SUMMARY

Radicals have been detected by means of ESR spectroscopy in γ -irradiated bromomalonamide and iodoacetamide. The radicals have been identified as CHBrCONH2 and CHICONH2, respectively. The ESR parameters and the geometries of each have been discussed in relation to other paramagnetic species in the halogen-substituted amide series. Some aspects of the Bromo- and iodo-radicals are characteristic of σ rather than π -electron radicals. The corresponding isotropic species of each, which conceivably could distinguish between the alternatives of σ or π radicals, proved elusive and were not obtained.



REFERENCES

PART I

- 1. P. C. Chieh, E. Subramanian and J. Trotter, J. Chem. Soc. A, 1970, 179.
- 2. H. N. Rexroad, Y. H. Hahn and W. J. Temple, <u>J. Chem. Phys.</u> 42, 324 (1965); N. Cyr and W. C. Lin, <u>Chem. Commun.</u> 1967, 192; <u>J. Chem. Phys.</u> 50, 3701 (1969).
- 3. D. C. Straw and G. C. Moulton, <u>J. Chem. Phys.</u> <u>57</u>, 2215 (1972).
- 4. E. M. Ayerst and J. R. C. Duke, <u>Acta Cryst</u>. 7, 588 (1954).
- 5. D. R. Davies and R. A. Pasternak, Acta Cryst. 9, 334 (1956).
- 6. J. A. Lerbscher, K. V. Krishna Rao, and J. R. Trotter, J. Chem. Soc. A 1971, 1505.
- 7. F. C. Phillips, An Introduction to Crystallography, New York: John Wiley, 1963, pp. 1,2.
- 8. J. Glusker and K. Trueblood, <u>Crystal Structure Analysis</u>:

 A Primer, New York: Oxford University Press, 1972,
 p. 186.
- 9. C. Kittel, <u>Introduction to Solid State Physics</u>. New York: John Wiley, 1971, p. 62.
- 10. International Tables for X-Ray Crystallography, Volume I, Birmingham: Kynoch Press, 1968.
- 11. M. J. Buerger, X-Ray Crystallography, New York: John Wiley, 1942, pp. 60-90.
- 12. International Tables for X-Ray Crystallography, Volume III. Birmingham: Kynoch Press, 1968.
- 13. J. Glusker and K. Trueblood, op. cit., p. 100.

- 14. P. Harker and J. S. Kasper, Acta Cryst. 1, 70 (1948).
- 15. D. Sayre, Acta Cryst. 5, 60 (1952).
- 16. J. Kapecki, <u>J. Chem. Educ</u>. 49, 231 (1972).
- 17. A. Kitaigorodskii, Organic Chemical Crystallography, New York: Consultants Bureau, 1955.
- 18. J. Backes, R. West and M. Whitely, <u>J. Chem. Soc.</u> 119, 359 (1921).
- 19. G. Glusker and K. Trueblood, op. cit., pp. 35-38.
- 20. M. J. Buerger, "The Photography of the Reciprocal Lattice," American Society of X-ray and Electron Diffraction Monograph, No. 1 (1944).
- 21. Program DATCOR, written by M. A. Neuman.
- 22. G. Stout and L. Jensen, X-Ray Structure Determination. New York: The MacMillan Co., 1968, p. 68
- 23. Program ABSCOR written by B-K. Lee and V. Day, modified and corrected by K. Knox, Rev. Sci. Instr. 38, 289 (1967) and adapted for the CDC 6500 computer.
- 24. Program PACK5 written by D. E. Williams.
- 25. Programs PATTR and FORO1 are part of Program CONNIE written by M. A. Neuman.
- 26. V. F. H. Schomaker and K. N. Trueblood, Acta Cryst. B24, 63 (1968); TLS modified to use MWCDC by M. Neuman, Amer. Crystallographic Society Meeting, Ames, Iowa (1971).
- 27. P. G. Jonsson and W. C. Hamilton, J. Chem. Phys. 56, 4433 (1972).

PART II

- 1. H. N. Rexroad, Y. H. Hahn and W. J. Temple, <u>J. Chem.</u>
 Phys. 42, 324 (1965).
- 2. N. Cyr and W. C. Lin, Chem. Commun. 1967, 192.
- 3. N. Cyr and W. C. Lin, J. Chem. Phys. 50, 3701 (1969)

- 4. D. C. Straw and G. C. Moulton, <u>J. Chem. Phys.</u> <u>57</u>, 2215 (1972).
- 5. M. Iwasaki, S. Noda, K. Toriyama, Mol. Phys. 18, 201 (1970).
- 6. F. Greenaway and M. T. Rogers, unpublished data.
- 7. F. Greenaway and M. T. Rogers, unpublished data.
- 8. M. T. Rogers and L. D. Kispert, <u>J. Chem. Phys.</u> 55, 2360 (1971), and references therein.
- 9. L. D. Kispert and M. T. Rogers, <u>J. Chem. Phys.</u> <u>54</u>, 3326 (1971).
- 10. A. Hudson and K. D. J. Root, Advances in Magnetic Resonance, Vol. 5, J. Waugh, Editor. New York: Academic Press, 1971.
- 11. R. P. Kohin, <u>J. Chem. Phys.</u> <u>50</u>, <u>5356</u> (1969); R. P. Kohin and R. S. Anderson, <u>Bull. Am. Phys. Soc.</u> <u>6</u>, 247 (1961).
- 12. L. D. Kispert and F. Myers, Jr., <u>J. Chem. Phys.</u> 56, 2623 (1972).
- 13. J. P. Michaut and J. Roncin, <u>Chem. Phys. Letters</u>, <u>12</u>, 95 (1971).
- 14. H. R. Falle, G. R. Luckhurst, A. Horsfield and M. Ballester, J. Chem. Phys. 50, 258 (1969).
- 15. M. Kashiwagi, Bull. Chem. Soc. Japan 39, 2051 (1966).
- 16. L. D. Kispert and M. T. Rogers, <u>J. Chem. Phys.</u> 58, 2065 (1973).
- G. W. Neilson and M. C. R. Symons, <u>J. Chem. Soc.</u> D 1973, 717
- 18. R. F. Picone and M. T. Rogers, unpublished results.
- 19. R. V. Lloyd and M. T. Rogers, unpublished results.
- 20. D. J. Edge and J. K. Kochi, <u>J. Amer. Chem. Soc.</u> 94, 6425 (1972).
- 21. T. Fujinaga, Y. Duguchi and K. Umemoto, Bull. Chem. Soc. Japan 37, 822 (1964); T. J. Kemp, G. T. Neal and T. J. Stone, J. Chem. Soc. A, 1969, 666; W. C. Danen, T. T. Kensler, J. G. Lawless, M. F. Marcus and M. D. Hawley, J. Phys. Chem. 77, 4389 (1969).

- 22. E. A. Lucken and C. Mazeline, <u>J. Chem. Phys.</u> 48, 1942 (1968).
- 23. J. R. Suttle and R. J. Lontz, <u>J. Chem. Phys.</u> 46, 1539 (1967).
- 24. L. D. Kispert, Abstracts of the 159th National Meeting of the American Chemical Society, PHYS 87, Houston, Texas, 1970.
- 25. C. R. Chen, H. J. Yue and D. W. Pratt, Chem. Phys. Letters
- 26. S. P. Mishra, G. W. Neilson and M. C. R. Symons, <u>J</u>. Amer. Chem. Soc. 95, 605 (1973).
- 27. G. W. Neilson and M. C. R. Symons, <u>J. Chem. Soc.</u> 1582 (1972).
- 28. R. J. Egland and J. E. Willard, <u>J. Phys. Chem.</u> 71, 4158 (1967); H. W. Fenrick, S. J. Filseth, A. L. Hanson and J. E. Willard, <u>J. Amer. Chem. Soc.</u> 85, 3731 (1963); R. J. Egland, P. J. Ogren and J. E. Willard, <u>J. Phys. Chem.</u> 75, 467 (1971).
- 29. J. Morton, Chem. Rev. 64, 453 (1964).
- 30. A. Carrington and H. Longuet-Higgins, Quart. Rev. 14, 427 (1960).
- 31. A. Carrington, Quart. Rev. 17, 67 (1963).
- 32. A. Carrington and A. McLachlan, <u>Introduction to Magnetic Resonance</u>. New York: Harper, 1970.
- 33. J. Wertz and J. Bolton, <u>Electron Spin Resonance</u>. New York: McGraw-Hill, 1972.
- 34. P. Ayscough, Electron Spin Resonance in Chemistry. London: Methuen, 1967.
- 35. C. Slichter, Principles of Magnetic Resonance. New York: Harper, 1963.
- 36. C. Poole, Jr. and H. Farach, Theory of Magnetic Resonance. New York: John Wiley, 1972.
- 37. A. Abragam and B. Bleaney, <u>Electron Paramagnetic Resonance of Transition Metal Ions</u>. London: Oxford University Press, 1970.
- 38. C. Poole, Jr., Electron Spin Resonance. New York: Interscience, 1967.

- 39. R. Alger, Electron Paramagnetic Resonance: Techniques and Applications. New York: Wiley, 1968.
- 40. B. Bleaney, Phil. Mag. 42, 441 (1951).
- 41. J. Swalen and H. Gladney, I.B.M. J., 515 (1964).
- 42. L. Rollmann and S. Chan, J. Chem. Phys. 50, 3416 (1969).
- 43. R. Lefebvre and J. Maruani, <u>J. Chem. Phys.</u> 42, 1480 (1965).
- 44. P. Krusic and J. Kochi, <u>J. Amer. Chem. Soc.</u> 90, 7155 (1968).
- 45. M. Symons, J. Amer. Chem. Soc. 91, 5924 (1969).
- 46. D. Wood and R. Lloyd, J. Chem. Phys. 53, 3922 (1970).
- 47. H. McConnell, J. Chem. Phys. 24, 764 (1956).
- 48. H. Fischer, Z. Naturforsch, 20a, 428 (1965).
- 49. S. I. Weissman, J. Chem. Phys. 25, 890 (1956).
- 50. R. Bersohn, J. Chem. Phys. 24, 1066 (1956).
- 51. H. McConnell, C. Heller, T. Cole and R. Fessenden, J. Amer. Chem. Soc. 82, 766 (1960).
- 52. N. Atherton, D. Whiffen, Mol. Phys. 4, 219 (1961).
- 53. M. T. Rogers and L. Kispert, <u>J. Chem. Phys.</u> <u>46</u>, 221 (1967).
- 54. J. Cook, J. Elliot and S. Wyard, Mol. Phys. 12, 185 (1967).
- 55. Y. Shioji, S. Ohnishi and K. Nitta, <u>J. Polymer Sci.</u> Pt. A. <u>1</u>, 3373 (1963).
- 56. P. Hamrick, Jr., H. Shields and S. Parkey, <u>J. Amer.</u> Chem. Soc. <u>90</u>, 5371 (1968).
- 57. A. Horsfield, J. Morton and D. Whiffen, Trans. Faraday Soc. 57, 1657 (1961).
- 58. J. Rowlands and D. Whiffen, Hyperfine Couplings. Teddington: National Physical Laboratory, 1961.
- 59. R. Cook, J. Rowlands, D. Whiffen, Mol. Phys. 7, 31 (1963).

- 60. M. T. Rogers and L. Kispert, <u>J. Chem. Phys.</u> 46, 3193 (1967).
- 61. M. T. Rogers and D. Whiffen, <u>J. Chem. Phys.</u> 42, 1955 (1964).
- 62. R. Lontz, <u>J. Chem. Phys.</u> 45, 1339 (1966).
- 63. F. Srygley and W. Gordy, J. Chem. Phys. 46, 2245 (1967).
- 64. K. Mobius, K. Hoffmann, M. Plato, Z. Naturforsch. 23a 1209 (1968).
- 65. J. Dejace, Acta Cryst. 8, 851 (1955).
- 66. J. Dejace, Bull. Soc. Franc. Miner. Crist., 13, (1959).
- 67. J. H. Mackey, M. Kopp and E. C. Tynan, in Electron Spin Resonance of Metal Complexes, edited by T. F. Yen New York: Plenum, 1969.
- 68. B. A. Goodman and J. B. Raynor, Advances in Inorganic Chemistry and Radiochemistry, 13, 135 (1970).
- 69. L. Pauling, <u>J. Chem. Phys.</u> 51, 2767 (1969); A. D. Walsh, <u>J. Chem. Soc.</u> 2301 (1953).
- 70. D. Schoemaker, Phys. Rev. 149, 693 (1966).
- 71. See, for example, R. S. Mulliken, C. A. Rieke, D. Orloff and H. Orloff, <u>J. Chem. Phys.</u> 17, 1248 (1949). We are indebted to Professor J. Harrison for computing the value for C-Br from Gaussian expansion of Slater orbitals.
- 72. R. F. Picone and M. T. Rogers, unpublished results.
- 73. E. A. C. Lucken, <u>Nuclear Quadrupole Coupling Constants</u>.

 New York: Academic Press, 1969
- 74. R. F. Picone, M. Neuman and M. T. Rogers, unpublished results.
- 75. W. G. Waller and M. T. Rogers, <u>J. Magn. Resonance</u> 9, 92 (1963).
- 76. R. F. Picone and M. T. Rogers, unpublished results.

